arXiv:astro-ph/0005112v2 28 Feb 2001

The Astrophysical Journal, 548: 564-584, 2001 February 20

A Determination of the Hubble Constant From Cepheid Distances and a Model of the Local Peculiar Velocity Field

Jeffrey A. Willick[1] & Puneet Batra

Stanford University, Department of Physics, Stanford, CA 94305

pbatra@perseus.stanford.edu

ABSTRACT

We present a measurement of the Hubble Constant based on Cepheid distances to 27 galaxies within 20 Mpc. We take the Cepheid data from published measurements by the Hubble Telescope Key Project on the Distance Scale (H_0KP). We calibrate the Cepheid Period-Luminosity (PL) relation with data from over 700 Cepheids in the LMC obtained by the OGLE collaboration; we assume an LMC distance modulus of 18.50 mag ($d_{\rm LMC} = 50.1$ kpc). Using this PL calibration we obtain new distances to the H_0KP galaxies. We correct the redshifts of these galaxies for peculiar velocities using two distinct velocity field models: the phenomenological model of Tonry et al. and a model based on the IRAS density field and linear gravitational instability theory. We combine the Cepheid distances with the corrected redshifts for the 27 galaxies to derive H_0, the Hubble constant. The results are $H_0 = 85 \pm 5$ km s^{-1} Mpc^{-1} (random error) at 95% confidence when the IRAS model is used, and 92 ± 5 km s^{-1} Mpc^{-1} when the phenomenological model is used. The IRAS model is a better fit to the data and the Hubble constant it returns is more reliable. Systematic error stems mainly from LMC distance uncertainty which is not directly addressed by this paper. Our value of H_0 is significantly larger than that quoted by the H_0KP, $H_0 = 71 \pm 6$ km s^{-1} Mpc^{-1}. Cepheid recalibration explains $\sim 30\%$ of this difference, velocity field analysis accounts for $\sim 70\%$. We discuss in detail possible reasons for this discrepancy and future study needed to resolve it.

Subject headings: cosmology — distance scale — galaxies

1. Introduction

A long-standing goal of observational cosmology is the measurement of the expansion rate of the universe, parameterized by the Hubble constant, H_0. Knowledge of H_0 enables us to assign galaxies absolute distances d from their redshifts cz,using $d = cz/H_0$, for $z \ll 1$. More fundamentally, the Hubble constant measures the time since the Big Bang, or the "expansion age" of the universe: $t_0 = f(\Omega_{\rm m}, \Omega_\Lambda) H_0^{-1}$, where $\Omega_{\rm m}$ and Ω_Λ are the density parameters for mass and the cosmological constant (or "dark energy"), respectively. The function $f(\Omega_{\rm m}, \Omega_\Lambda)$ has well known limiting values $f = 2/3$ for $\Omega_{\rm m} = 1$ and $f = 1$ for $\Omega_{\rm m} = 0$, if $\Omega_\Lambda = 0$. In the flat ($\Omega_{\rm m} + \Omega_\Lambda = 1$) models now favored by CMB anisotropy measurements (e.g., Tegmark & Zaldarriaga 2000; Lange et al. 2000), f is larger, at given $\Omega_{\rm m}$, than in the $\Omega_\Lambda = 0$ case. However, unless $\Omega_{\rm m} \lesssim 0.25$, which is disfavored by a variety of data (Primack 2000), $f \leq 1$, even in a flat universe. It follows that for currently acceptable values of the density parameters, the expansion age of the universe is $\lesssim H_0^{-1}$.

[1]Deceased.

By convention, extragalactic distances are measured in Mpc, redshifts in $\mathrm{km\,s^{-1}}$, and H_0 in $\mathrm{km\,s^{-1}\,Mpc^{-1}}$. From the mid-1960s through the mid-1980s, two groups dominated the debate over H_0. One, associated mainly with Sandage and collaborators, argued that $H_0 = 50\,\mathrm{km\,s^{-1}\,Mpc^{-1}}$ with relatively small ($\sim$ 10%) uncertainty. A second, led by de Vaucouleurs, advocated $H_0 = 100\,\mathrm{km\,s^{-1}\,Mpc^{-1}}$ with similarly small error. The corresponding values of the expansion timescale are $H_0^{-1} = 9.8\,h^{-1}$ Gyr, where $h \equiv H_0/100\,\mathrm{km\,s^{-1}\,Mpc^{-1}}$. Thus, the large Hubble constant favored by de Vaucouleurs leads to a "young" ($t_0 \lesssim 10$ Gyr) universe, while the small H_0 favored by Sandage corresponds to an "old" ($t_0 \gtrsim 15$ Gyr) universe. In recent years, the debate has shifted, with many groups finding H_0 to be intermediate between the Sandage and de Vaucouleurs values. Especially important in this regard has been the work of the Hubble Space Telescope (HST) Key Project on the Extragalactic Distance Scale (H_0KP), which finds $H_0 = 71 \pm 6\,\mathrm{km\,s^{-1}\,Mpc^{-1}}$ (Mould et al. 2000). We discuss their methods and results further below.

An independent constraint on the age of the universe comes from the age of the oldest stars t_*. This can be measured from the turnoff point in the Hertzsprung-Russell diagrams of old globular clusters. The best current estimates (Krauss 1999; see also Caretta et al. 1999) suggest that $t_* = 12.8 \pm 1.0$ Gyr ($1\,\sigma$ error), and that $10 \leq t_* \leq 17$ Gyr at 95% confidence. If one furthermore assumes that the globular clusters did not form until about $\Delta t \sim 1$ Gyr after the Big Bang, then the age of the universe as indicated by the oldest stars is $t_* + \Delta t \approx 14 \pm 1$ Gyr. With the above estimates, we thus require that t_0 be strictly larger than 10 Gyr, and prefer that it be $\gtrsim 13$ Gyr, to ensure consistency of the Big Bang model with stellar ages.

From this perspective, the de Vaucouleurs value of H_0 yields far too small an expansion time, while the Sandage value produces one that is comfortably large. The current modern value (H_0KP) gives a marginally consistent $t_0 = 13.3 \pm 1.3$ Gyr if we assume an $\Omega_\mathrm{m} = 0.3$, $\Omega_\Lambda = 0.7$ universe as preferred by a variety of present data. A Hubble constant only 20% larger, however, would give an expansion age of 10.6 Gyr, and thus conflict with the best estimates of the globular cluster ages.

The determination of the Hubble constant clearly remains a crucial part of the cosmological puzzle. Recent efforts by the H_0KP and other groups have greatly reduced the allowed range for H_0, but have not unequivocally demonstrated consistency between the timescales of Big Bang cosmology and stellar evolution. The main purpose of this paper is to underscore the importance of ongoing work on the problem, by presenting an alternative approach, using existing data, to measuring H_0. The outline of this paper is as follows: In §2 we discuss the effects of peculiar velocities on the determination of H_0, and strategies for overcoming these effects. In §3 we present a derivation of the Cepheid PL relation using the Optical Gravitational Lensing Experiment (OGLE; Udalski et al. 1999a,b) database of LMC Cepheids, and in §4 we apply the new PL relation to the H_0KP Cepheid database to obtain distances for the H_0KP galaxies. In §5 we constrain the local peculiar velocity field by applying the maximum likelihood VELMOD method to a sample of galaxies with accurate relative distances from surface brightness fluctuations. In §6 we apply the resulting velocity models to the H_0KP Cepheid galaxies, and thereby obtain a value of H_0. In §7 we further discuss and summarize our results.

2. Peculiar velocities and the strategies for measuring H_0

Measuring H_0 requires addressing the effects of peculiar velocities—those deviations from the underlying Hubble flow. The observed redshift cz of a galaxy at a distance d is given by $cz = H_0 d + u$, where u is the radial component of its peculiar velocity. In the (unfortunately) hypothetical case of pure Hubble flow ($u \equiv 0$), a few good distance and redshift measurements of very nearby galaxies would cleanly yield H_0.

Over the last two decades, however, it has become clear that galactic peculiar velocities are both substantial ($\sim$ several hundred $\mathrm{km\,s^{-1}}$) and *systematic,* i.e., coherent over volumes of diameter $\sim$ 10–20 Mpc (see Willick 2000 for a recent review). Neglecting peculiar velocities can produce an error $\delta H_0/H_0 \sim u/cz$ for

a single galaxy, while observing N galaxies does not necessarily lead to a $\sqrt{N}$ reduction due to the coherence of the velocity field. H_0 measurement errors due to uncorrected peculiar velocities can approach $\sim 30\%$ at redshifts as large as ~ 1500 km s^{-1}, roughly the distance to the Virgo cluster, even if moderately large ($N \sim 10$) samples are used.

At least two straightforward paradigms exist to handle the impact on H_0 from peculiar velocities: In the first approach (*Method I*), one measures H_0 in the "far field" of the Hubble flow—peculiar velocities here are washed out in comparison with the large expansion velocities $H_0 d$. In the second approach (*Method II*), one measures H_0 in the "near field" of the Hubble flow after using an accurate model of the local pecuilar velocity field $u(\mathbf{r})$ to prune the observed redshifts cz of their peculiar velocity contributions.

Method I requires no knowledge of peculiar velocities, provided they are fractionally small. At redshifts beyond ~ 5000 km s^{-1}, for example, the fractional uncertainty in the Hubble constant, u/cz, will generally be $< 10\%$ for a single galaxy. Method I does, however, require data at distances where it is difficult or impossible to directly employ primary distance indicators such as Cepheids. Instead, secondary distance indicators, such as the Tully-Fisher relation or the Surface Brightness Fluctuation method (SBF), must be used. Not only are secondary DI's less intrinsically accurate than Cepheids, but they also lack *a priori* absolute calibrations. This motivates a first look at how sources of error in the calibration process and distance scale relatively impact Method I and Method II analyses.

Primarily, uncertainty in the absolute calibration of the Cepheid PL relation, (itself due to uncertainty in the distance to the LMC), floods the systematic uncertainty in H_0. As Gibson (1999) has emphasized, values as small as $\mu_{\rm LMC} = 18.2$ mag and as large as $\mu_{\rm LMC} = 18.7$ mag have appeared recently in the literature, though H_0KP adopts $\mu_{\rm LMC} = 18.50$ mag. H_0 estimates could be revised upwards by as much as 15% if the smallest LMC distances prove correct, or downward by as much as 10% should the largest LMC distance hold.

Also, a recalibration of the Cepheid P-L relation is desired because the current P-L relation used by the H_0KP is based on only 32 Cepheids in the LMC (Ferrarese et al. 2000b) while the OGLE has found many more. The H_0KP is also in the process of redetermining Cepheid galaxy distances using a calibration based on the OGLE data (W. Freedman, private communication; Madore & Freedman 2000, in preparation). Our own work with the OGLE data (see §4) indicates that the actual Cepheid distances are systematically $\sim 5\%$ shorter than the distances originally used by the HOKP.

These Cepheid uncertainties will propagate through any Method I *or* II approach that uses the Cepheid

Table 1. Tonry et al. calibration of the SBF distance scale

Galaxy	$\overline{m_I^0}$ (mag)	μ_{ceph}[a] (mag)	$\overline{M_I}$ (mag)
NGC0224	22.67 ± 0.06	24.44 ± 0.10	-1.77 ± 0.12
NGC3031	26.21 ± 0.25	27.80 ± 0.08	-1.59 ± 0.26
NGC3368	28.34 ± 0.21	30.20 ± 0.10	-1.86 ± 0.23
NGC4548	29.68 ± 0.54	31.04 ± 0.08	-1.36 ± 0.55
NGC4725	28.87 ± 0.34	30.57 ± 0.08	-1.70 ± 0.35
NGC7331	28.85 ± 0.16	30.89 ± 0.10	-2.04 ± 0.19

[a]From Ferrarese et al. 2000a

distance scale. The extent of this propagation motivates our choice of method. Method II approaches cut the propagation chain and use these Cepheid distances directly. Method I approaches use this Cepheid distance scale to calibrate a secondary distance scale, as mentioned above, which then provides the distances used to measure H_0. We focus on those Method I approaches that use Surface Brightness Fluctuations (SBF; Tonry & Schneider 1988) as the secondary distance indicator to highlight the difficulties in the calibration process and offer a first motivation toward Method II approaches. Ferrarese et al. (2000a) give a more exhaustive review of the calibration process in other secondary distance indicators.

Table 1 shows the tabulated SBF calibration data from Tonry et al. (2000; hereafter TBAD00). Column 1 lists the 6 galaxy names for which both color-adjusted SBF apparent bulge magnitudes ($\overline{m_I}$; Column 2) and Cepheid-based distance moduli (μ_{ceph}; Column 3) are available.

Table 1 reveals a spread in $\overline{M_I}$ of $\sim$ .8 mag, with half of the measured values within the estimated systematic error of .16 mag of the H_0KP SBF zero point, -1.79 mag (Ferrarese et al. 2000a), and the Tonry et al. (TBAD00) zero-point of -1.74 mag. Both values agree with the theoretically predicted value, -1.81 mag (Worthey 1993); the H_0KP value leads to a distance scale that is in good agreement with other secondary distance scales (Ferrarese et al. 2000a).

The SBF and Cepheid Virgo distances indicate that the preferred calibration of Tonry et al. (TBAD00), as well as the similar H_0KP calibration (Ferrarese et al. 2000a), is inconsistent with our revised Cepheid distance scale. As noted in (§4) the mean Cepheid distance to the five Virgo galaxies considered in this paper is 14.7 Mpc. If only the three galaxies within the canonical 6 degrees of the Virgo center are considered, this rises to 15 Mpc. By comparison, the mean SBF distance, using the Tonry et al. calibration above, of 27 Virgo galaxies in the SBF sample is 16.5 Mpc. If the SBF zero point, formerly in agreement with theory and other distance indicators, were shifted to bring the SBF Virgo galaxies to the 15 Mpc value suggested by the Cepheids, the value for H_0 derived from the analyses of TBAD00 and Blakeslee et al. (1999; see §5) would rise by $\sim 7\%$, while the H_0KP value would rise by $\sim 10\%$, close to the upper edge of the (Cepheid + SBF) systematic error envelope. This new result would still depend critically on the 6 calibrating galaxies of Table 1. As illustrated, the inevitable errors in the Cepheid calibration propagate directly into the secondary distance calibration, and the derived H_0.

The main advantage of Method II over Method I is that no such intermediate calibration step is required. One uses only the primary distances from Cepheid variables, which are more reliable within ~ 2000 km s^{-1}, but still subject to uncertainties. The disadvantage of Method II is that it requires an accurate model of the local peculiar velocity field. Turner, Cen & Ostriker (1992) performed theoretical analyses of the impact a lack of an accurate velocity field would have on local measures of H_0; constructing a satisfactory model has proved difficult but possible, as we discuss below. However, any systematic errors in the model result in errors in the corrected redshifts, and thus in the derived Hubble constant. The gains of removing the systematics from secondary calibration are countered by the velocity field systematics.

In the past decade Method I has taken precedence in Hubble constant determinations. The H_0KP, in particular, has adopted the philosophy of Method I, focusing its efforts on determining Cepheid distances to galaxies that can serve as suitable calibrators for secondary distance indicators. As the foregoing discussion indicates, however, the two approaches emphasize different systematic effects, and should each be employed as mutual checks. We attempt in this paper to redress the imbalance by applying Method II. Our approach has been made possible by the advent of data sets that allow the local velocity field to be more accurately modeled than previously, as we discuss in detail in §5.

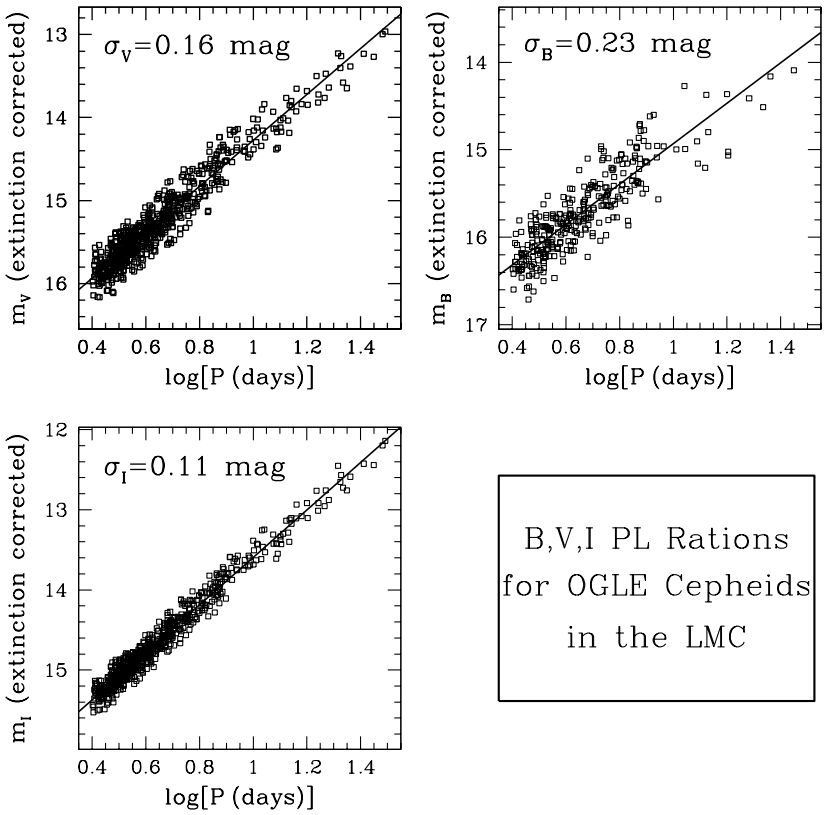

Fig. 1.— B (top right), V (top left), and I (lower left) band PL relations for Cepheid variables found by the OGLE experiment in the Large Magellanic Cloud. The solid lines are linear fits to the data.

3. Recalibration of the Cepheid Period-Luminosity Relation

In §4 we will derive distances to the H_0KP sample. First, however, we perform the recalibration of the Cepheid PL relation discussed in §2, based on the OGLE data.

The OGLE project has monitored fields in the LMC nearly every clear night for the last three years. Its primary goal was to detect gravitational lensing events; however, in the course of this monitoring, the OGLE discovered more than 1300 Cepheid variable stars in the LMC.[2] Of these, a majority are fundamental mode pulsators of the sort observed by the H_0KP in more distant galaxies. We use a subsample of the OGLE Cepheids judged by Udalski et al. (1999a) to be fundamental mode pulsators, and that have periods greater than 2.5 days, to calibrate the I and V band PL relations. Cepheids with shorter periods may not be fundamental mode pulsators, and moreover are not present in the H_0KP data set which contains only luminous Cepheids. There are 729 such stars in the OGLE catalog. Of these, 331 also have B band data, and we use this subset to calibrate the B band PL relation. This latter calibration is for reference only, however, as the H_0KP data consists only of V and I band Cepheid data.

We correct the observed Cepheid mean magnitudes for total extinction, Galactic plus LMC, as deter-

[2]The OGLE catalog of Cepheid variables in the LMC is publicly available at http://astro.princeton.edu/ogle/ogle2/var_stars/lmc/cep/catalog.

mined by the reddenings for each field given by Udalski et al. (1999b). We adopt the ratios of extinction to reddening, $R_X \equiv A_X/E(B-V)$ (where $X = B$,V,I) given by Schlegel, Finkbeiner, & Davis (1998; SFD). These values are given in Table 2. We then fit a linear apparent magnitude versus log period relation in each of the three bandpasses:

$$m_X = a_X + b_X \log P\,. \tag{1}$$

The extinction corrected magnitudes are plotted versus $\log P$ in Figure 1. The solid lines show the best-fit PL relation for each bandpass. The parameters a_X and b_X, along with related information, are given in Table 2. Outliers were eliminated by iterating the fit several times and excluding objects which deviated by more than 2.5σ. The final fit parameters are those obtained after this iterative procedure converged. The number of objects used in the final fit is given in Table 2 as N_{fit}, as compared with the quantity N_{tot}, the total number of data points in the given bandpass meeting the initial cut on $\log P$. The exclusion of outliers is justified because of the likelihood of contamination of the sample by first-overtone Cepheids (see Udalski et al. 1999a for further details).

3.1. Absolute Calibration of the Cepheid PL Relation

The apparent magnitude-log period relations given in Table 2 need to be converted into absolute PL relations in order to use them as distance indicators for other galaxies. To do this, we must adopt a distance modulus for the LMC, $\mu_{\rm LMC}$. The LMC distance has been a contentious issue and remains, perhaps, the greatest source of systematic uncertainty in the extraglactic distance scale (Ferrarese et al. 2000b). Recent determinations of $\mu_{\rm LMC}$ (see Gibson 1999 for a review) have ranged from $\mu_{\rm LMC} = 18.20 \pm 0.05$ (Popowski & Gould 1998; Stanek, Zaritsky, & Harris 1998; Udalski et al. 1998a,b) to $\mu_{\rm LMC} = 18.55 \pm 0.05$ (Cioni et al. 2000; Hoyle, Shanks, & Tanvir 2000). We will follow the H_0KP and adopt $\mu_{\rm LMC} = 18.50$. Although this may be somewhat higher than the mean of recent measurements, we believe it is the conservative choice for now. In any case, our ultimate Hubble constant scales in a simple way with $\mu_{\rm LMC}$, and can be adjusted accordingly should the LMC distance become better determined in the future.

Using $\mu_{\rm LMC} \equiv 18.50$, the absolute Cepheid PL relations follow directly from the parameters given in Table 2. We write our final PL relations in the form

$$M_X = A_X + b_X(\log P - 1)\,. \tag{2}$$

We thus set the zero point at $P = 10$ d, corresponding to a "typical" fundamental mode Cepheid. Comparison of Eqs. (1) and (2) shows that $A_X = a_X + b_X - 18.5$ for our adopted value of $\mu_{\rm LMC}$. The PL slopes are of course the same. We thus obtain the final parameters for the Cepheid PL relations shown in columns (2) and (3) of Table 3. The slope errors are the same as those given in Table 2; we do not tabulate zero point errors because they are completely dominated by the ~ 0.2 mag systematic uncertainty in the LMC distance modulus.

Table 2. The OGLE LMC Cepheid Apparent PL Relations

Band	R_X	a_X	b_X	σ (mag)	N_{fit}	N_{tot}
I	1.96	16.557 ± 0.014	-2.963 ± 0.021	0.108	658	729
V	3.24	17.041 ± 0.021	-2.760 ± 0.031	0.159	650	729
B	4.32	17.240 ± 0.049	-2.308 ± 0.073	0.235	310	331

It is useful to compare these PL parameters to those obtained from a completely separate sample: Cepheids from the Hipparcos database with parallax distances. Obviously, the latter are unaffected by the distance to the LMC, although they have other problems, such as incompleteness and potential systematic parallax errors. Lanoix, Paturel, & Garnier (1999b) have calibrated the PL relation for 174 Cepheids with Hipparcos parallaxes and have obtained the zero point and slope given in columns (3) and (4) of Table 3. As can be seen, there is excellent agreement to within the Hipparcos-based errors of the PL zero points. The V band slopes are in similarly excellent agreement. The I band slopes agree less well, but it is difficult to gauge the significance of the disagreement because Lanoix et al. (1999b) do not give slope errors. In any case, because $\log P = 1$ is a typical extragalactic period, the slope difference will not translate into a large predicted absolute magnitude difference. Hence we can say with confidence that the OGLE-based PL relations from the LMC are in good agreement with the PL relations derived from Galactic Cepheids with Hipparcos parallaxes. This argues against a large ($\gtrsim 0.2$ mag) error in our adopted LMC distance modulus.

4. Distances to Cepheid Galaxies

We apply the OGLE PL relations given in Table 2 to a sample of thirty-four galaxies for which V and I band Cepheid data are available from the H_0KP team and two other groups. It is supplemented by a small number of Cepheids with ground-based V and I band data. All the data were acquired from the electronic archive maintained by P. Lanoix at the URL `http://www-obs.univ-lyon1.fr/~planoix/ECD`; See Lanoix et al. (1999a) for more details.

Basic data for the thirty-four galaxies, listed in order of increasing heliocentric redshift, are given in Table 4. The names, in Column 1, are those preferred by Lanoix. Galactic longitude (ℓ, Column 2) and latitude (b, Column 3) and heliocentric redshift ($cz_\odot$, Column 4) were all obtained from the NASA Extragalactic Database (NED; `http://nedwww.ipac.caltech.edu`). For reference we also list the Local Group (LG) frame and CMB frame redshifts, $cz_{\rm LG}$ and $cz_{\rm CMB}$, in Columns 5 and 6. Galactic reddenings $E(B-V)$ determined by SFD (also obtained from NED) are listed in Column 7.[3] Column 8 lists the number of Cepheids in each galaxy for which V and I band PL data are available.

Further references for each galaxy are given in column 9 of Table 4. Seven galaxies are denoted "LG," indicating that they are members of the LG according to the compilation of Mateo (1998).[4] The V and I

[3]The SFD reddenings represent the effects of Galactic dust only, and therefore are not suitable for correcting the Cepheid magnitudes for extinction, which is often dominated by extinction within the *host* galaxy. We do not use the SFD reddenings in any case, but present them here for completeness.

[4]For all seven we obtain Cepheid distances (see Table 5) smaller than 1.5 Mpc, and for four of them we obtain distances less

Table 3. Cepheid PL Relations ($\mu_{LMC} = 18.5$ mag)

Band	A_X	b_X	A_X	b_X
	OGLE		Hipparcos[a]	
I	-4.906	-2.963	-4.86 ± 0.09	-3.05
V	-4.219	-2.760	-4.21 ± 0.05	-2.77
B	-3.569	-2.308	...	...

[a]Lanoix et al.

Table 4. List of Cepheid Galaxies

Name	ℓ (deg)	b (deg)	$cz_{\odot}$ ($\mathrm{km\,s^{-1}}$)	cz_{LG} ($\mathrm{km\,s^{-1}}$)	cz_{CMB} ($\mathrm{km\,s^{-1}}$)	$E(B-V)$ (mag)	N_{ceph}	Notes
NGC 224	121.17	−21.57	−300	−13	−584	0.062	37	LG (M31)
IC 1613	129.72	−60.58	−234	−65	−558	0.025	10	LG
NGC 598	133.61	−31.33	−179	70	−459	0.042	12	LG (M33)
NGC 6822	25.34	−18.39	−57	7	−262	0.240	6	LG
NGC 3031	142.09	40.90	−34	126	46	0.080	25	H_0KP (M81)
NGC 300	299.21	−79.42	144	126	−89	0.013	16	F92
NGC 5457	102.04	59.77	241	362	360	0.009	33	H_0KP (M101)
SEXTANS B	233.20	43.78	301	139	642	0.032	3	LG
IC 4182	107.70	79.09	321	342	548	0.014	28	SS/KP
SEXTANS A	246.15	39.88	324	117	678	0.044	7	LG
NGC 3109	262.10	23.07	403	129	736	0.067	16	LG
NGC 5253	314.86	30.11	404	156	678	0.056	7	SS/KP
NGC 4258	138.32	68.84	448	505	651	0.016	15	Maoz/KP
NGC 4548	285.69	76.83	486	380	805	0.038	24	H_0KP (M91)
NGC 925	144.89	−25.17	553	781	326	0.076	79	H_0KP
NGC 2541	170.18	33.48	559	645	694	0.050	34	H_0KP
NGC 3198	171.22	54.83	663	703	879	0.012	52	H_0KP
NGC 4414	174.54	83.18	716	691	988	0.019	11	H_0KP
NGC 3621	281.21	26.10	727	437	1059	0.080	69	H_0KP
NGC 3627	241.96	64.42	727	597	1072	0.032	36	SS/KP
NGC 3319	175.98	59.34	739	758	978	0.015	28	H_0KP
NGC 3351	233.95	56.37	778	640	1123	0.028	49	H_0KP (M95)
NGC 7331	93.72	−20.72	816	1110	492	0.091	13	H_0KP
NGC 3368	234.44	57.01	897	760	1242	0.025	11	T/KP
NGC 2090	239.46	−27.43	931	758	1002	0.040	34	H_0KP
NGC 4639	294.30	75.99	1010	901	1328	0.026	17	SS/KP
NGC 4725	295.08	88.36	1206	1160	1486	0.012	20	H_0KP
NGC 1425	227.52	−52.60	1512	1442	1413	0.013	29	H_0KP
NGC 4321	271.14	76.90	1571	1467	1893	0.026	52	H_0KP (M100)
NGC 1365	237.96	−54.60	1636	1546	1539	0.020	52	H_0KP
NGC 4496A	290.56	66.33	1730	1573	2070	0.025	94	SS/KP
NGC 4536	292.95	64.73	1808	1645	2148	0.018	39	SS/KP
NGC 1326A	238.55	−56.28	1836	1750	1730	0.017	17	H_0KP
NGC 4535	290.07	70.64	1961	1825	2293	0.019	50	H_0KP

band data compiled by Lanoix for these objects are ground-based. The LG galaxies are included here for completeness, but are not used in the H_0 determination presented in §6. Galaxies in the LG have no leverage on H_0 because their Hubble velocities are negligible in comparison with random peculiar motions.

Of the 27 remaining objects, all of which are used in the H_0 analysis in §6, 26 have HST data. The one exception is NGC 300, which has ground-based data from Freedman et al. (1992; F92). PL data for this galaxy in the Lanoix database that are *not* from F92 are not used in our analysis.

For the twenty-six galaxies with HST data, eighteen were observed originally by the H_0KP team. These objects are denoted "H_0KP" in Table 4. The complete Cepheid database for these galaxies, as well as a detailed compendium of publications by the H_0KP, is given at the Key Project website.[5] A further seven galaxies were originally observed by other HST investigators: six by the Sandage/Saha (Saha et al. 1999) group, and one by Tanvir et al. (1995), denoted "SS/KP" and "T/KP" respectively, in Table 4. The data for all seven were subsequently reanalyzed by the H_0KP team (Gibson et al. 2000). We use *only* the reanalyzed data from these seven galaxies in order to ensure uniformity with the rest of the H_0KP analyzed data that we use. Finally, one galaxy, NGC 4258, is denoted "Maoz/KP" in Table 4. It is not formally part of the H_0KP sample, but was observed with the HST by Maoz et al. (1999), in collaboration with members of the H_0KP team, in order to compare Cepheid distances with the highly accurate maser distance of Herrnstein et al. (1999; we discuss this special case further in §7). The Cepheid data for NGC 4258 are as yet unpublished, but were kindly provided to us in advance of publication by J. Newman. They are also available in Lanoix's database.

4.1. Calculation of Distances

We determine the distance to each galaxy by minimizing a χ^2 statistic that measures deviations from the V and I band PL relations. The statistic is minimized with respect to variations in the galaxy distance modulus μ and the total reddening, Galactic plus internal, along the line of sight toward each Cepheid in the galaxy. We also assumed a single reddening value for all stars in the galaxy. This led to an identical value of the distance modulus but a much higher value of the PL scatter, indicating that the reddening is variable across the face of each galaxy.

Suppose we have PL data for $i = 1, ..., N_{\rm Ceph}$ Cepheids in the galaxy in question, with one V band and one I band mean magnitude, and one period, for each star. Let m_{ij}, where $j = V, I$, denote the magnitudes, and $X_i = \log P_i$, where P_i is the pulsation period in days, of the ith star. The appropriate χ^2 statistic is then

$$\chi^2 = \sum_{i=1}^{N_{\rm Ceph}} \sum_{j=V,I} \left[m_{ij} - (A_j + b_j(X_j - 1) + \mu + R_j E(B-V)_i) \right]^2 / \sigma^2 \,. \qquad (3)$$

Minimization of χ^2 yields the distance modulus μ and the $N_{\rm Ceph}$ reddenings $E(B-V)_i$. The PL parameters for the two bandpasses are hardwired to the values given in Table 3.

When we minimize this χ^2 statistic for each of the 34 galaxies listed in Table 4, we obtain the distance moduli, and the corresponding distances in Mpc, given in Table 5. We discuss the calculation of uncertainties below. We do not tabulate the reddenings for each star here, although this information can be made available electronically to interested readers. We do, however, list the mean reddenings, $\langle E(B-V) \rangle$, for each galaxy in Table 5. We note that, to within the errors, these reddenings are consistent with being

than 0.8 Mpc. Our distances agree with those given by Mateo (1998) to within the errors.

[5]The Key project web site can be found at `www.ipac.caltech.edu/`H_0`KP`. The Lanoix database includes this database as a subset; a crosscheck confirms that the periods and magnitudes in the two are identical.

Table 5. Cepheid Galaxy Distances

Name	μ (mag)	d (Mpc)	$\langle E(B-V)\rangle$ (mag)
NGC224	24.37 ± 0.07	0.75 ± 0.03	0.202 ± 0.027
IC1613	24.29 ± 0.14	0.72 ± 0.05	0.085 ± 0.052
NGC598	24.47 ± 0.13	0.78 ± 0.05	0.223 ± 0.048
NGC6822	23.27 ± 0.18	0.45 ± 0.04	0.337 ± 0.067
NGC3031	27.66 ± 0.09	3.40 ± 0.14	0.138 ± 0.033
NGC300	26.55 ± 0.12	2.04 ± 0.11	0.026 ± 0.043
NGC5457	29.20 ± 0.08	6.91 ± 0.25	0.081 ± 0.029
SEXB	25.80 ± 0.26	1.45 ± 0.17	$-.029 \pm 0.095$
IC4182	28.27 ± 0.08	4.50 ± 0.17	0.016 ± 0.031
SEXA	25.74 ± 0.17	1.41 ± 0.11	0.060 ± 0.062
NGC3109	25.27 ± 0.12	1.13 ± 0.06	0.137 ± 0.043
NGC5253	27.53 ± 0.17	3.21 ± 0.25	0.143 ± 0.062
NGC4258	29.49 ± 0.12	7.90 ± 0.42	0.128 ± 0.043
NGC4548	30.94 ± 0.09	15.38 ± 0.64	0.118 ± 0.034
NGC925	29.78 ± 0.05	9.04 ± 0.21	0.168 ± 0.019
NGC2541	30.32 ± 0.08	11.58 ± 0.41	0.137 ± 0.028
NGC3198	30.71 ± 0.06	13.84 ± 0.39	0.101 ± 0.023
NGC4414	31.17 ± 0.13	17.13 ± 1.06	0.113 ± 0.050
NGC3621	29.10 ± 0.05	6.62 ± 0.16	0.260 ± 0.020
NGC3627	29.70 ± 0.07	8.73 ± 0.30	0.188 ± 0.027
NGC3319	30.70 ± 0.08	13.83 ± 0.53	0.083 ± 0.031
NGC3351	29.91 ± 0.06	9.59 ± 0.28	0.166 ± 0.024
NGC7331	30.79 ± 0.12	14.39 ± 0.82	0.196 ± 0.046
NGC3368	29.94 ± 0.13	9.72 ± 0.60	0.155 ± 0.050
NGC2090	30.30 ± 0.08	11.47 ± 0.40	0.124 ± 0.028
NGC4639	31.58 ± 0.11	20.69 ± 1.03	0.117 ± 0.040
NGC4725	30.37 ± 0.10	11.87 ± 0.54	0.212 ± 0.037
NGC1425	31.60 ± 0.08	20.93 ± 0.79	0.114 ± 0.031
NGC4321	30.80 ± 0.06	14.48 ± 0.41	0.141 ± 0.023
NGC1365	31.26 ± 0.06	17.83 ± 0.51	0.140 ± 0.023
NGC4496A	30.80 ± 0.05	14.43 ± 0.30	0.107 ± 0.017
NGC4536	30.77 ± 0.07	14.24 ± 0.47	0.133 ± 0.026
NGC1326A	31.07 ± 0.11	16.36 ± 0.81	0.096 ± 0.040
NGC4535	30.88 ± 0.06	15.02 ± 0.43	0.132 ± 0.023

larger than the SFD Galactic reddenings given in Table 4. When the reddening errors are sufficiently small for an estimate to be made—typically, when $N_{\rm Ceph} \gtrsim 30$—we find that the mean *internal* reddening, $\langle E(B-V)_{int} \rangle = \langle E(B-V) \rangle - E(B-V)_{SFD98}$, is of order 0.1 mag.

Once a galaxy distance modulus and the $N_{\rm Ceph}$ reddenings are determined, one may calculate V and I band absolute magnitudes for each star as follows:

$$M_{i,j} = m_{ij} - R_j E(B-V)_i - \mu \,, \tag{4}$$

where $i = 1, ..., N_{\rm Ceph}$ and $j = V, I$. The PL relation for the entire sample may then be exhibited as a plot of $M_{i,j}$ versus $\log P_i$ for all stars in all galaxies, as shown in Figure 2. A total of 1021 stars is plotted in the Figure. The OGLE PL relations given in Table 3 are plotted through the points as dotted lines. Note that the V band PL relation has smaller scatter than the I band relation. In fact, the scatter visible in the plots is smaller than the true scatter, because the fits have one degree of freedom, the reddening, for each star (plus one for each galaxy).

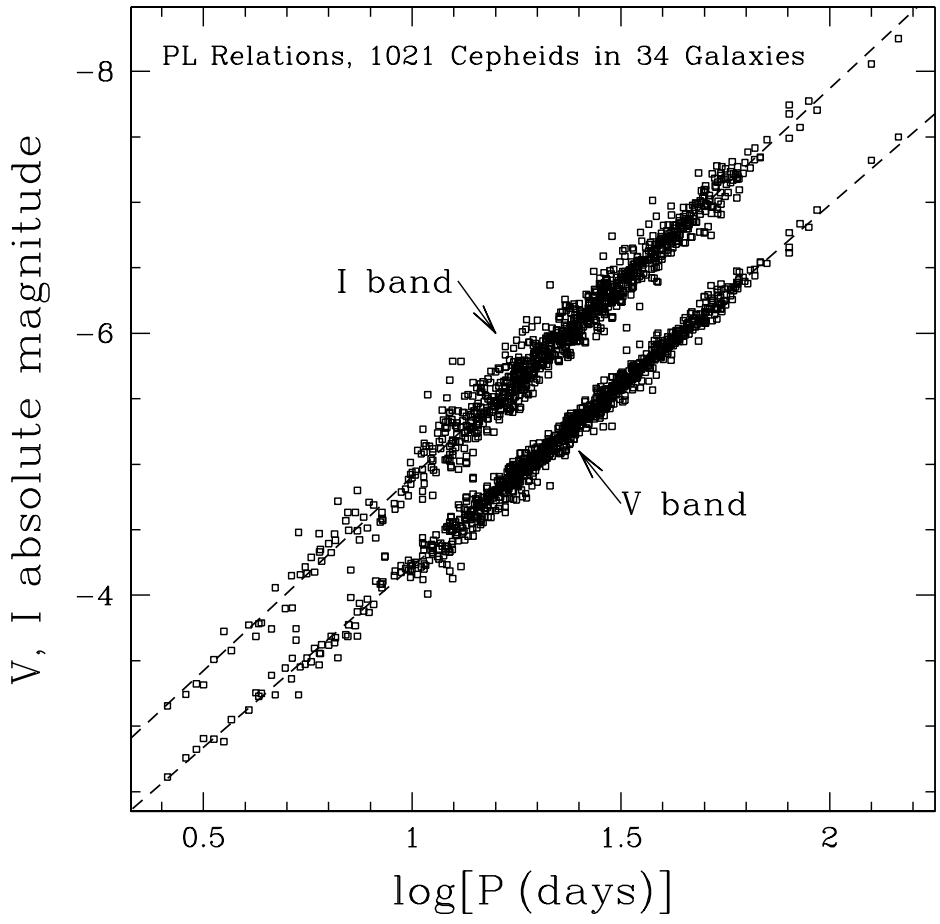

Fig. 2.— $V-$ and $I-$ band PL relations for the 1021 Cepheids in the 34-galaxy sample described in Table 4. The periods are the measured ones, while the absolute magnitudes are calculated using Eq. (4). The dotted lines show the OGLE PL calibrations given in Table 3.

When these degrees of freedom are properly taken into account, the PL scatters for the 1021 Cepheids are

$$\begin{aligned} \sigma_V &= 0.111 \quad \mathrm{mag} \\ \sigma_I &= 0.165 \quad \mathrm{mag}\,. \end{aligned} \tag{5}$$

These scatters are similar to those derived from the LMC fit (Table 2), although there it was the I band scatter that was smaller. This most likely reflects the fact that in the LMC fit the reddenings were given a priori, and reddening errors increase the V band PL residuals more than I band residuals. Taken together, the LMC and 34-galaxy sample results suggest that the V and I band PL scatters are about the same in the absence of extinction, and that $\sigma_V \approx \sigma_I \approx \sigma_{\rm Ceph} = 0.15$ mag. We assume that this approximation holds for the remainder of the paper. Our method for calculating random distance errors for the Cepheid galaxies is given in Appendix A.

5. Fitting Velocity Field Models

In order to use the Cepheid galaxies to estimate the Hubble constant, we must, as explained in § 2, use an accurate model of the local velocity field. We employ two quite different models in this paper:

1. An IRAS model, in which peculiar velocities are based on the distribution of galaxies in the nearby universe ($cz \lesssim 10,000$ km s^{-1}) as determined by the 1.2 Jy IRAS redshift survey (Strauss et al. 1992; Fisher et al. 1995). The velocity field is then a function of the parameter $\beta \equiv \Omega_{\rm m}^{0.6}/b$, where b is the biasing factor for IRAS galaxies. Before applying the model the IRAS model to the Cepheids, then, we must first determine the appropriate value(s) of β to use.
2. A phenomenological model, in which the local velocity field is dominated by a few simple components. We adopt a model of the form recently used by TBAD00, which includes a dipole, a quadrupole, and two "attractors," one centered on the Virgo Cluster and one on the Great Attractor (GA). This model has a large number of free parameters, whose values must be determined before the model can be applied to the Cepheids.

Each of the two models has strong and weak points. The IRAS model is more realistic and is better motivated physically. *All* mass fluctuations in the local universe, not only prominent attractors, affect the velocity field, as they must if structure grows from gravitational instability. However, the IRAS model suffers from undercounting early-type galaxies in clusters, and thus may well underestimate the importance of massive concentrations such as Virgo and the GA. In contrast, the Tonry (TBAD00) model allows one to ascribe as much influence on the velocity field to Virgo and the GA as the data warrant. However, because it includes *only* these attractors, the Tonry model may attribute greater or lesser importance to these than they would have in reality to compensate for missing mass concentrations and voids.

The fact that each model is imperfect suggests that the prudent approach is to try both. In what follows, we first describe (§5.1) our method for fitting velocity models. We next describe (§5.2) the 281 galaxy Surface Brightness Fluctuation (SBF) data set to which we fit each of the two models and comment on a key difference between our treatment of this data set and previous treatments. After that we present (§5.3) the constraints that the SBF data set allows us to place on the IRAS model (i.e., the allowed values of β and several ancillary parameters to be described), and (§5.4) the best-fitting parameters of the phenomenological Tonry model.

5.1. The VELMOD Method

For both optimizing our peculiar velocity models with the SBF data, and for determining H_0 with the Cepheid data (in §6), we use the VELMOD maximum likelihood approach. The method was described in

detail in two papers (Willick et al. 1997b, hereafter WSDK; Willick & Strauss 1998, hereafter WS), so we limit ourselves to a brief overview here. When we fit a peculiar velocity model to redshift-distance data, two sources of variance enter in: distance measurement error and small-scale velocity noise. The latter is the part of the the peculiar velocity field that cannot be predicted by any model. It results from close gravitational encounters with other galaxies in groups, rather than from the systematic pull of the large-scale gravity field. When velocity models are fit to relatively distant ($\gtrsim 30h^{-1}\,$Mpc) galaxies, the distance errors ($\lesssim 10\%$ for SBF or Cepheid distances, $\sim 20\%$ for Tully-Fisher distances) dominate. However, at the much smaller distances of interest here ($\lesssim 20h^{-1}\,$Mpc), the velocity noise is equal to or larger than distance errors. Thus, it is essential that we calibrate it properly.

VELMOD was designed with precisely this aim. It is based on the explicit expression for the probability that a galaxy along a given line of sight has a measured distance d and redshift cz :

$$P(\ln d, cz; \mathbf{p}) \propto \int_0^\infty r^2 n(r) P(\ln d|r) P(cz|r)\, dr\,, \tag{6}$$

where r is the *true* (as opposed to measured) distance along the line of sight, and $\mathbf{p}$ is a vector of parameters that determine the model peculiar velocity field. Here and in what follows, we assume that r and d are measured in units of $\mathrm{km\,s^{-1}}$, i.e., we take $H_0 \equiv 1$. We will drop this assumption only in the last step of the analysis, when we apply VELMOD to the Cepheid sample to determine H_0. In Eq. (6), $n(r)$ is the number density of galaxies at distance r along the line of sight,

$$P(\ln d|r) = \frac{1}{\sqrt{2\pi}\Delta} \exp\left\{-\frac{[\ln(d/r)]^2}{2\Delta^2}\right\}\,, \tag{7}$$

where $\Delta = 0.46\delta\mu$ is the fractional distance error, $\delta\mu$ is the distance modulus error, and

$$P(cz|r; \mathbf{p}) = \frac{1}{\sqrt{2\pi}\sigma_v(r)} \exp\left\{-\frac{(cz - [r + u(r)])^2}{2\sigma_v(r)^2}\right\}\,, \tag{8}$$

where $\sigma_v(r)$ is the velocity noise and $u(r)$ the radial component of the predicted velocity field. Note that we allow σ_v to vary with position; in practice we can also allow it (in the case of the IRAS model) to vary with local number density. Of course, $u(r)$, $\sigma_v(r)$, and $n(r)$ depend on the parameter vector $\mathbf{p}$.

Eq. (6), the joint probability distribution of distance and redshift, is not the optimal quantity on which to base likelihood-maximization because it is quite sensitive to the density as well as the velocity model. It is more suitable to use the conditional probability,

$$P(\ln d|cz; \mathbf{p}) = \frac{P(\ln d, cz)}{\int_0^\infty P(\ln d, cz)\, d(\ln d)} = \frac{\int_0^\infty r^2 n(r) P(\ln d|r) P(cz|r)\, dr}{\int_0^\infty r^2 n(r) P(cz|r)\, dr}\,, \tag{9}$$

which is less sensitive to the density model because of the presence of $n(r)$ in both numerator and denominator. The conditional probability that the $i = 1, ..., N$ sample galaxies have observed distances d_i given that their redshifts are cz_i is then

$$P(\mathrm{data}; \mathbf{p}) = \prod_{i=1}^{N} P(\ln d_i|cz_i; \mathbf{p})\,. \tag{10}$$

The essential step in VELMOD is maximizing the above sample probability with respect to the model parameter vector $\mathbf{p}$. In practice, this is done by minimizing the statistic

$$\mathcal{L} = -2 \ln P(\mathrm{data}; \mathbf{p})\,. \tag{11}$$

WSDK showed using simulated data sets that minimizing $\mathcal{L}$, as defined by Eqs. (9) through (11), recovers unbiased values of velocity model parameters.

5.2. The SBF Sample

The best current data set to use for constraining the local peculiar velocity field is the SBF sample of Tonry and collaborators (Tonry et al. 1997, 2001). The full sample comprises ~ 300 early-type (mainly E and S0) galaxies out to $\sim 4000\ \mathrm{km\,s^{-1}}$, although most are within $\sim 3000\ \mathrm{km\,s^{-1}}$. For our fitting, we use a subset of the sample consisting of 281 galaxies that are not in the LG, have $(V-I)$ colors > 0.9, and are consistent with our velocity models at the $\leq 3\,\sigma$ level. The SBF distances are accurate in most cases to $\lesssim 10\%$. This accuracy is considerably better than what is available for Tully-Fisher samples; moreover, the SBF method yields a reliable distance *error* estimate for each galaxy, whereas for Tully-Fisher one generally has only a global scatter which is itself somewhat uncertain. Having a good distance error estimate is crucial if the velocity noise information is to be properly incorporated into the VELMOD procedure.

TBAD00 and Blakeslee et al. (1999) have already used the SBF sample to fit local velocity models. The former study fit the phenomenological model mentioned above, and the latter an IRAS model, to the SBF distances. Neither study, however, used the VELMOD method per se. Tonry et al. used a related approach, one that accounted for small-scale velocity dispersion but not for the role of the volume element (the r^2 term in §5.1) or of density variations (the $n(r)$ term in §5.1). Blakeslee et al. employed the same method that Davis, Nusser, & Willick (1996) used to fit a Tully-Fisher sample at larger distances; as this approach does not fully account for the effects of velocity noise, it is less suitable for the nearby flow field analysis that is of greatest importance here. In what follows, we borrow from both the TBAD00 and the Blakelee et al. (1999) studies, in that we employ similar models of the velocity field, but we use the VELMOD method in order to treat effects neglected in those papers.

Unlike TBAD00 and Blakeslee et al. (1999), we do not assume an absolute calibration of the SBF relation. That is, we use the SBF data only as indicators of distances in $\mathrm{km\,s^{-1}}$, not in Mpc. Specifically, Tonry et al. and Blakeslee et al. took the SBF relation to be

$$\overline{M_I} = -1.74 - 4.5(V-I)\,, \tag{12}$$

where $\overline{M_I}$ is the mean fluctuation absolute magnitude of a galaxy of a given $(V-I)$ color. They then assign an absolute distance $d_{abs} = 10^{\left[0.2(\overline{m_I}-\overline{M_I})-5\right]}$ Mpc to a galaxy with measured apparent fluctuation magnitude $\overline{m_I}$. Consequently, when they fit their velocity models, one of the unknown free parameters is necessarily the Hubble constant[6]. In contrast, we write the SBF relation

$$\overline{M_I} = A - 4.5(V-I)\,, \tag{13}$$

where A is a free parameter in our maximum likelihood analysis, and then compute SBF distances in $\mathrm{km\,s^{-1}}$ according to $d = 10^{\left[0.2(\overline{m_I}-\overline{M_I})\right]}$; it is this value of d that enters into calculation of the probability, Eq. (9). Because we never convert SBF distances to Mpc, *our analysis of the velocity field using the SBF data does not yield a value for, and is completely unrelated to, the value of the Hubble constant.* That is, no assumptions concerning the distance scale go into our velocity field analysis; it is only later, when we apply the VELMOD method to the Cepheid galaxies, that absolute distances enter our analysis. Therefore, it is only the Cepheid distances themselves that directly affect the value of the Hubble constant. (We emphasize, however, that we adopt the Tonry et al. SBF slope (4.5) as well as their reported distance errors in our analysis.)

It should be noted that our use of a relative rather than an absolute zero point, while conceptually important, is largely a technical distinction. The values of H_0 obtained by Tonry et al. and Blakeslee et al. are entirely dependent on their specific choice of SBF zero point in Eq. (12), and this value is not very well determined (see Tonry et al. 1997 for an in-depth discussion). A different choice of zero point would have

[6]Indeed, TBAD00 reported $H_0 = 77 \pm 4\ \mathrm{km\,s^{-1}\,Mpc^{-1}}$ and Blakelee et al. (1999) reported $H_0 = 74 \pm 4\ \mathrm{km\,s^{-1}\,Mpc^{-1}}$ (random errors) in addition to their constraints on the velocity field.

led Tonry et al. and Blakelee et al. to find a different H_0, but not a different velocity field. Our approach simply makes this explicit by removing absolute distances altogether from the problem of determining the velocity field.

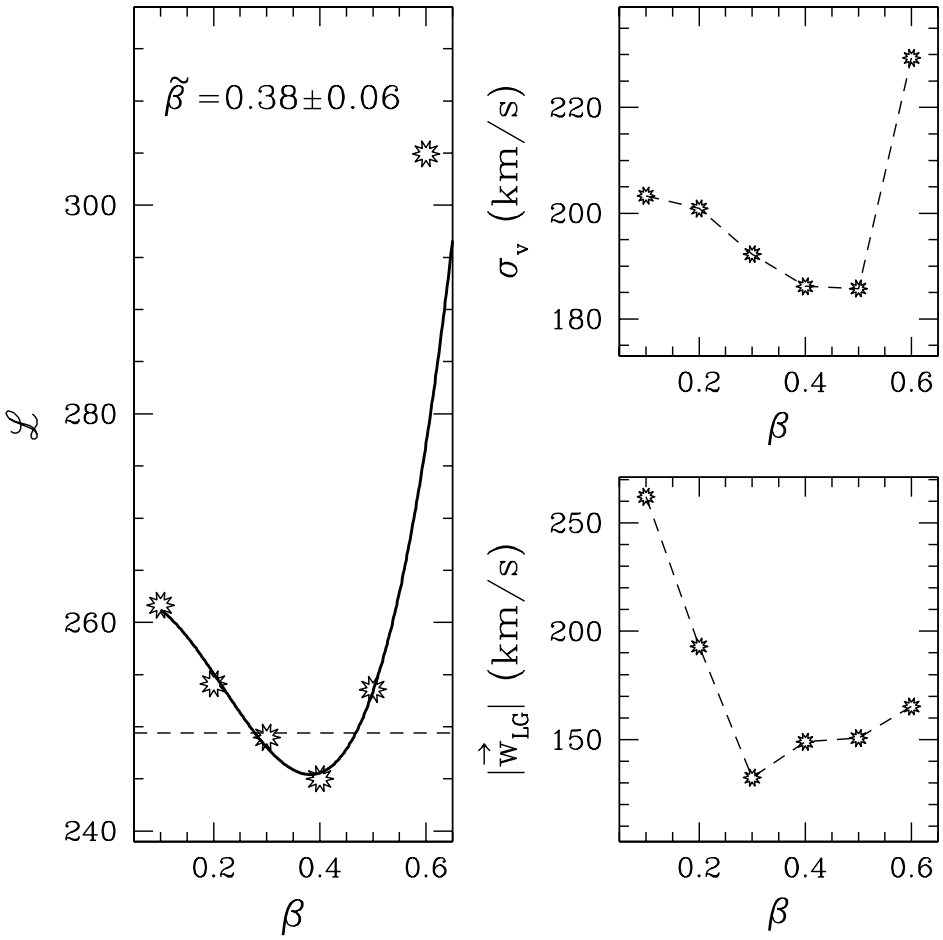

Fig. 3.— *Left*: The points show the VELMOD likelihood statistic $\mathcal{L}$ versus β for the SBF sample and the linear, 300 km s^{-1}-smoothed IRAS velocity field (see text for details). The solid line shows a cubic fit to the points for $0.1 \leq \beta \leq 0.5$. The minimum of the curve yields the maximum likelihood value of β and its uncertainty, as indicated on the figure. The horizontal dashed line shows the 2σ confidence limits on β. *Top right*: the maximum-likelihood value of the velocity noise σ_v versus β. *Bottom right*: Maximum-likelihood value of the Local Group velocity amplitude, $|\mathbf{w}_{LG}|$, relative to the IRAS predictions.

5.3. The IRAS Model

There are any number of "IRAS models" one can apply because, aside from the obvious question of the value of β, there are the issues of smoothing scale, filtering, nonlinear corrections to the velocity-density relation, etc. The range of possibilities was discussed by WSDK and WS, to which readers are referred for a detailed discussion of the relative merits of each. Tests in those papers with Tully-Fisher data, and with the SBF data (Willick, Narayanan, Strauss, & Blakeslee, in preparation; hereafter WNSB), have demonstrated clearly that the smallest possible Gaussian smoothing scale for the IRAS data, 300 km s^{-1}, yields the most

accurate velocity field (see Berlind, Narayanan, & Weinberg 2000 for a theoretical justification of this fact). A second outcome of such tests is that the best fits to both the Tully-Fisher and SBF data are obtained when the linear theory velocity-density relation,

$$\mathbf{v}(\mathbf{r}) = \frac{\beta}{4\pi} \int d^3\mathbf{r}' \, \frac{\delta_g(\mathbf{r}')(\mathbf{r}' - \mathbf{r})}{|\mathbf{r}' - \mathbf{r}|^3} \,, \tag{14}$$

is used, where δ_g is the density contrast of IRAS galaxies smoothed on a 300 $\mathrm{km\,s^{-1}}$ scale. Proposed modifications to Eq. (14) to account for nonlinear dynamics, as well as hypothesized nonlinear biasing relations, have not yet been shown to improve the fit, although they typically increase the best value of β by $\sim 10\%$. The reasons for this are unclear at present, but will be discussed in depth by WNSB. For now, we use the linear theory, 300 $\mathrm{km\,s^{-1}}$ smoothed IRAS velocity field based on Eq. (14).[7]

Figure 3 shows the main results of applying VELMOD to the SBF data set using the linear IRAS velocity field. The $\mathcal{L}$ versus β plot shows a strong minimum (likelihood maximum) near $\beta = 0.4$; the solid curve is a cubic fit to the likelihood points, and its minimum determines the maximum likelihood value of β and its $1\,\sigma$ uncertainty: $\beta = 0.38 \pm 0.06$. The $\beta = 0.3$ likelihood lies within 4 units of $\mathcal{L}$ from the minimum and is thus acceptable at the $2\,\sigma$ level, while the $\beta = 0.2$ and $\beta = 0.5$ models are about $3\,\sigma$ away from the maximum likelihood value. Note that $\beta > 0.5$ is ruled out with very high confidence. Indeed, we do not plot results for $\beta > 0.6$ since the likelihood is so poor. These results suggest that we apply the $\beta = 0.2, 0.3, 0.4$, and 0.5 IRAS models to the Cepheid galaxies when we determine H_0 below, giving the most weight to the $\beta = 0.3$ and $\beta = 0.4$ results.

As is standard for IRAS VELMOD (WSKD), we also allow for a random motion of the LG $\mathbf{w}_{\rm LG}$ with respect to the IRAS prediction, which is treated as a free parameter. As found by WSKD and WS, this velocity is generally small $\lesssim 150$ $\mathrm{km\,s^{-1}}$ for β near its optimum value. This result is confirmed here in the lower right panel of Figure 3. The upper right panel shows the variation of the final free parameter, the velocity noise σ_v, with β. It, too, generally minimizes near the maximum likelihood β, and this occurs here as well. However, note that σ_v has a considerably larger value, ~ 185 $\mathrm{km\,s^{-1}}$, for the best fit model than was found in the Tully-Fisher VELMOD fits of WS and WSKD, where $\sigma_v \approx 130$–150 $\mathrm{km\,s^{-1}}$ was a more typical value. It is probable that this reflects a real difference between the small-scale velocity noise for late-type (Tully-Fisher) and early-type (SBF) galaxies; we will address this issue in WNSB. When we apply the IRAS (and Tonry) models to the Cepheid galaxies in §6, we will use values of σ_v typical of the Tully-Fisher spirals, rather than the large σ_v found here.

As discussed by WSDK and WS, a good method for visually assessing the quality of the IRAS velocity model is to compute smoothed velocity residuals for the sample (see, e.g., Eq. (9) of WS for details on how such residuals are calculated). Sky plots of such residuals are presented in Figure 4 for the $\beta = 0.4$ model. The Gaussian smoothing scale employed rises from 250 $\mathrm{km\,s^{-1}}$ at $cz \lesssim 500$ $\mathrm{km\,s^{-1}}$ to 700 $\mathrm{km\,s^{-1}}$ at 3500 $\mathrm{km\,s^{-1}}$; thus, the smoothed residuals will exhibit coherence over $\sim 30^\circ$ scales. Coherence on larger scales than this signifies a failure of the model.

The residuals in Figure 4 are essentially incoherent on large scales, as indicated by the fact that both starred (outflowing) and open (inflowing) symbols are well mixed throughout the plots. Furthermore, the amplitude of these velocity residuals is almost everywhere $\lesssim 100$ $\mathrm{km\,s^{-1}}$, and is in many places virtually zero (indicated by the smallest points on the figure). These aspects of Figure 4 indicate that the IRAS model provides a good fit to the SBF data. The open squares in Figure 4 indicate the positions of the Cepheid galaxies to which the IRAS and Tonry models will be applied in §5. The squares are seen to lie in regions well sampled by the SBF data, so that the velocity models are well-constrained where the Cepheid galaxies are found.

[7] In the language of WSDK and WS, we note that our adopted model also employs Wiener filtering and Method IV.

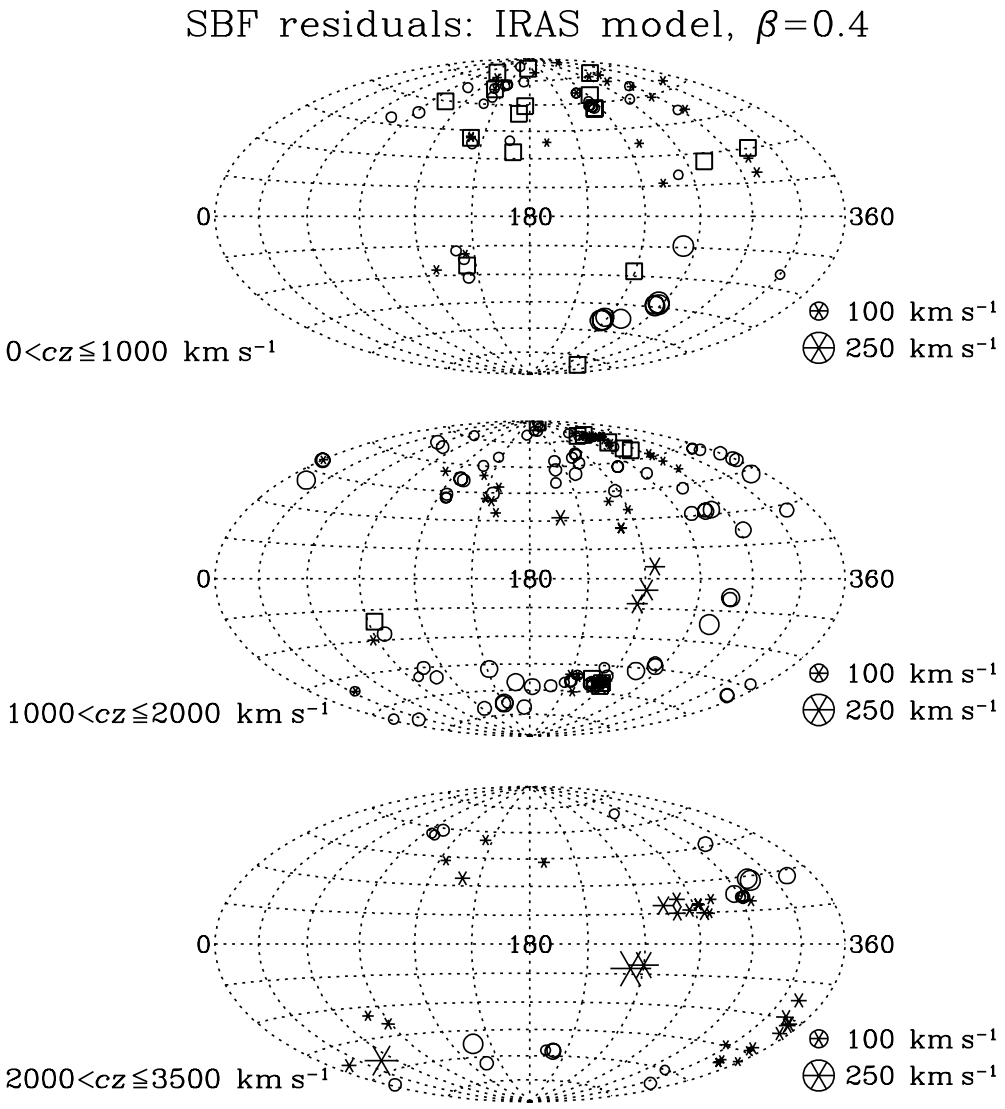

Fig. 4.— Smoothed peculiar velocity residuals of the SBF galaxies relative to the IRAS-predicted velocities, for $\beta = 0.4$. Stars represent objects with positive radial peculiar velocity relative to the IRAS model, and open circles objects with negative peculiar velocity relative to IRAS. The open squares show the positions of the 27 Cepheid galaxies used to determine H_0.

There is one region, however, where a conspicuous failure of the IRAS model seems to occur: in the lower right quadrant of the $cz \leq 1000$ km s^{-1} map. A group of six SBF galaxies appear to have a coherent flow at ~ 150 km s^{-1} relative to the IRAS model there. However, this pattern does not continue into the next redshift interval, where there are more Cepheid galaxies and where the leverage on the H_0 measurement is greater. Consequently, we do not attempt to correct for this apparent failure of the IRAS model (the Tonry model shows the same discrepancy). However, this anomaly remains unexplained and deserves further attention.

5.4. The Tonry Model

Our phenomenological model has the same functional form as the TBAD00 model. However, we have implemented the model in a system of units in which distance is measured in $\mathrm{km\,s^{-1}}$, and used the VELMOD formalism, which differs in a number of ways (§5.1, Batra & Willick 2000) from that of TBAD00. To maximize independence from the IRAS results, we assume $n(r) =$ constant in Eqs. (6) and (9) when we implement the Tonry model.

An important distinction between the Tonry model and the IRAS models is that the former is carried out entirely in the CMB reference frame, i.e., the redshifts used are $cz_{\rm CMB}$, whereas for the IRAS models $cz_{\rm LG}$ is used. The frame of reference is a highly nontrivial issue for local velocity field fits, as redshifts can differ by up to 600 $\mathrm{km\,s^{-1}}$ (Table 4, Courteau & van den Bergh 1999). It is thus important to demonstrate that comparable results can be obtained regardless of frame.[8]

The Tonry model assumes the local peculiar velocity field to be dominated by two spherically symmetric attractors, one centered on the Virgo Cluster and one on the Great Attractor. Each attractor is taken to have a mean interior overdensity given by

$$\delta(r) = \frac{\delta_0 e^{-r/R_{cut}}}{1-\gamma/3}\left(\frac{r}{R_c}\right)^{-3}\left[\left(1+(r/R_c)^3\right)^{1-\gamma/3}-1\right] \tag{15}$$

where r is the distance from the center of the attractor. Note that the attractors have both a "cutoff" radius R_{cut} and a "core" radius R_c. Each attractor produces an infall velocity given by the Yahil's (1985) expression,

$$v_{in}(r) = \frac{1}{3}\Omega_{\rm m}^{0.6} r\,\delta(r)\left[1+\delta(r)\right]^{-1/4} \tag{16}$$

The value of $\Omega_{\rm m}$ is not well constrained by the fit, being highly covariant with δ_0 (TBAD00), and it thus suffices to fix it at an arbitrary value, which we take to be 0.2.

To roughly account for the effects of mass inhomogeneities other than the attractors, the model also includes velocity dipole and quadrupole fields; the latter is exponentially truncated and centered on the LG. These fields are added vectorially to the infall velocities produced by the attractors.

We fit the Tonry model to the SBF data set, allowing some, but not all, of the model parameters to vary. As discussed in detail by TBAD00, there is significant covariance among the parameters, so to simplify the fit we take the attractor core radii R_c and power-law exponents γ to have the TBAD00 values. The model also contains the velocity dispersions of the tracer galaxies as a function of position (i.e., the quantity $\sigma_v(r)$ in Eq. (8)). TBAD00 took the background dispersion to be 187 $\mathrm{km\,s^{-1}}$, and then added this value in quadrature with an additional dispersion, σ_v^{core}, within a distance R_c of three clusters: Virgo, the Great Attractor, and Fornax. For these dispersions, too, we adopted the TBAD00 values. (Note, however, that Fornax does not contribute to the overall velocity field.)

Table 6 presents our best fit values for the parameters we allowed to vary, as well as those held fixed at the TBAD00 values. Those parameters which denote positions in space are given in Supergalactic coordinates, in $\mathrm{km\,s^{-1}}$ units. For this table, the dipole components, in $\mathrm{km\,s^{-1}}$, are $(-70, 230, -40)$; the quadrupole matrix is

$$\begin{pmatrix} 1.79 & 2.17 & -6.62 \\ 2.17 & -10.5 & -3.99 \\ -6.62 & -3.99 & 8.71 \end{pmatrix}. \tag{17}$$

[8]One can also implement the Tonry model in the LG frame. We have done this, and the value of H_0 we obtain is unchanged.

5.4.1. *Comparison of Velocity Models*

Figure 5 provides a comparison of the IRAS and Tonry models along the lines of sight toward four SBF galaxies that lie in regions that are also important for the Cepheid analysis of §6. We plot both our own fit of the Tonry model to the SBF data (solid line) and that of TBAD00 (dotted line). Peculiar velocity in the LG frame is plotted as a function of Hubble-flow distance. The IRAS velocity field generally exhibits more "features," i.e., it is not as smooth as the Tonry models. This results from the fact that the IRAS peculiar velocity field is produced by all mass fluctuations, while the phenomenological model assumes only the existence of two attractors. Another important difference is in the different strength of the Virgo (NGC 4476) and Great (NGC 4616) Attractors. The IRAS velocity field exhibits relatively weak gradients ($|u'(r)| \lesssim 0.5$ near Virgo, $|u'(r)| \lesssim 0.25$ near the Great Attractor), while the Tonry model has large gradients ($|u'(r)| \gtrsim 1$) in these regions. The greater influence of the attractors arises because, in the Tonry model, they must account for all features of the velocity field, some of which are in reality due to other mass fluctuations. (On the other hand, the mild gradients in the IRAS $u(r)$ near Virgo may be due in part to the undercounting of cluster galaxies by IRAS.) As we shall see §6, the Tonry model does not fit the Cepheid data as well as the IRAS model; as a result, we shall, in the end, adopt the value of H_0 derived from the IRAS model.

6. Application of the Velocity Models to the Cepheid Galaxy Sample

In this section we apply the velocity models of §5 to the Cepheid galaxy sample discussed in §4. Our application is limited to the twenty-seven galaxies listed in Tables 4 and 5 that are not LG members. As noted in §4, 26 of these 27 galaxies have HST Cepheid data that have been analyzed by the H_0KP team; the one galaxy for which ground-based data are used, NGC 300, was analyzed by H_0KP team members (Freedman et al. 1992) and is thus expected to be on the same system. The Cepheid sample used here thus constitutes a uniform data set.

We now apply the VELMOD method to the Cepheid data set, as we did in §5 for the SBF data; here we determine H_0. There is now one key difference: the Cepheid galaxy distances d are in Mpc, and correspondingly, Eq. (7) is rewritten

$$P(\ln d|r) = \frac{1}{\sqrt{2\pi}\Delta} \exp\left\{ -\frac{[\ln(H_0 d/r)]^2}{2\Delta^2} \right\} . \tag{18}$$

In the exercise of §5 a vector of free parameters, **p**, on which the velocity model depended, was varied to maximize likelihood. Now, **p** is held fixed at the values determined in §5—i.e., the same velocity field is used—and the only parameter that is varied to maximize likelihood is H_0. Aside from these differences, the VELMOD procedure applied to the Cepheid galaxies is identical to that applied to the SBF data set.

Table 6. Best-fit parameters of Tonry Model

Attractor	(x,y,z) ($\mathrm{km\,s^{-1}}$)	σ_v[a] ($\mathrm{km\,s^{-1}}$)	δ_0	R_{cut} ($\mathrm{km\,s^{-1}}$)	γ[a]	R_c[a] ($\mathrm{km\,s^{-1}}$)
Virgo	$(-250, 1300, -140)$	650	54.7	968	1.5	157
GA	$(-2950, 1170, -1370)$	500	179.4	4010	2.0	157
Fornax	$(-150, 1180, -1050)$	235	N/A	N/A	N/A	157

[a]Parameter held fixed at the TBAD00 value.

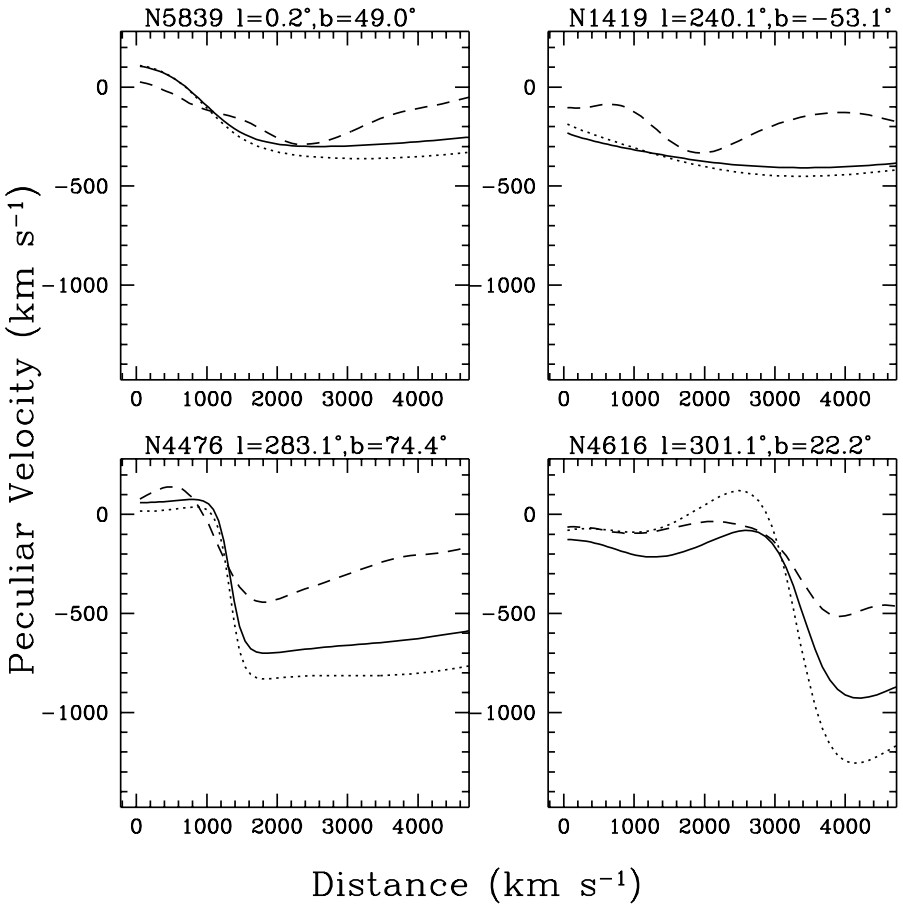

Fig. 5.— Comparison of predicted peculiar velocities along the line of sight for four selected galaxies. The dashed line represents the IRAS model, the solid line shows our redetermination of the Tonry model, and the dotted line the TBAD00 model itself.

6.1. Results from the IRAS models

To apply the IRAS model we must adopt a functional form and value of $\sigma_v(r)$, the small-scale velocity noise as a function of position. Following WS, we write

$$\sigma_v(r) = \sigma_{v,0} + f_v \delta_g(r), \tag{19}$$

where δ_g is the IRAS galaxy overdensity at position r along the line of sight. Thus, $\sigma_{v,0}$ is the velocity noise in a mean-density environment, and f_v represents the rate of increase of velocity dispersion with density, an effect expected on theoretical grounds and verified in N-body simulations (Kepner, Summers, & Strauss 1997; Strauss, Ostriker, & Cen 1998). For the Cepheid sample we adopt $\sigma_{v,0} = 135$ km s^{-1} and $f_v = 30$ km s^{-1}, similar to the values WSDK and WS found for Tully-Fisher VELMOD. As noted earlier, this value of σ_v is considerably smaller than the ~ 185 km s^{-1} found for the SBF sample, but the Cepheid galaxies are late-type spirals and are more likely to resemble the Tully-Fisher galaxies in their dynamical properties.

There is one subset of galaxies within the Cepheid sample that are not well-described by this model of $\sigma_v(r)$, namely, Virgo cluster members. Virgo's relatively high (~ 650 km s^{-1}) velocity dispersion cannot be matched by the linear increase with density at the IRAS smoothing scale of 300 km s^{-1}. To account for

this we "collapse" Virgo, following WS and WSDK—i.e., we set the redshift of each Virgo galaxy to its mean value of $cz_{\rm LG,Virg} = 1035\ {\rm km\,s^{-1}}$ (Huchra 1985). To account for uncertainty in this value, we set the $\sigma_v = 30\ {\rm km\,s^{-1}}$ for each collapsed Virgo galaxy. The Cepheid galaxies deemed likely Virgo members were NGC4536, NGC4321, NGC4496A, NGC4535, and NGC4548. Their mean Cepheid distance is 14.7 Mpc. The distance of each one is within $\sim 1.5\sigma$ of this mean value, each is within 10° of the Virgo core at $\ell = 283.8°$, $b = 74.5°$, and each has a redshift within 700 ${\rm km\,s^{-1}}$ of the Virgo mean. Thus, these are all strong candidates for Virgo membership, and collapsing them significantly improves the fit likelihood. However, as we now show, whether or not we collapse Virgo makes little difference to the derived value of H_0.

Table 7 presents the main results of applying the IRAS velocity models to the Cepheid sample. Column 1 lists the value of β (the values of $\mathbf{w}_{\rm LG}$ used are always those derived from the SBF fit at that value of β, and $\sigma_v(r)$ is always given as discussed in the previous paragraph); Column 2 lists the maximum likelihood value of H_0 and its $1\,\sigma$ uncertainty; columns 3 and 4 give the values of the likelihood statistic $\mathcal{L}$ and a χ^2 for the fit, which is discussed further below. Columns 5, 6, and 7 repeat the information of 3, 4, and 5 for the case that Virgo is not collapsed, i.e., when the true LG redshifts of the Virgo galaxies are used in the likelihood analysis.

The most striking feature of Table 7 is the robustness of H_0 with respect to changes in β. Indeed, the results of the Table can be summarized by the statement $H_0 = 85 \pm 2.5\ {\rm km\,s^{-1}\,Mpc^{-1}}$ at 65% ($1\,\sigma$) confidence, irrespective of the value of β, provided it is in the range 0.2–0.5 that is allowed by the IRAS velocity model applied to the SBF sample.[9] When Virgo is not collapsed, the likelihood statistics and χ^2 values indicate a much worse fit. This occurs because the Virgo galaxy redshifts scatter so widely about the mean cluster value, and our simple model of velocity noise increase with density does not account for this (possibly because the huge central densities are smoothed out, and because IRAS undercounts cluster cores). It is important to note, however, that not collapsing Virgo affects the derived value of H_0 very little, increasing it by an amount about equal to the $1\,\sigma$ error estimate. Thus our treatment of Virgo is not crucial to the main conclusion of this paper.

We discuss below the calculation of the confidence intervals on H_0. First, we describe the calculation of the χ^2 statistics listed in Table 7.

[9]The application of VELMOD to Tully-Fisher samples by WSDK and WS preferred higher values of β, in the range 0.4–0.6 at 95% confidence. We consider the SBF result to be more reliable because of the greater precision of SBF distances. In any case, we note that $\beta = 0.4$ is allowed by both the SBF and Tully-Fisher data, and thus constitutes the preferred value at present.

Table 7. Solutions for IRAS Velocity Fields

	Virgo Collapsed			No Virgo Collapse		
β	H_0 ($\rm km\,s^{-1}\,Mpc^{-1}$)	$\mathcal{L}$	χ^2	H_0 ($\rm km\,s^{-1}\,Mpc^{-1}$)	$\mathcal{L}$	χ^2
0.2	84.9 ± 1.6	34.7	44.7	85.6 ± 2.4	68.0	79.9
0.3	84.6 ± 1.9	31.6	38.8	86.4 ± 2.5	62.1	72.8
0.4	85.3 ± 2.2	35.5	39.4	87.5 ± 2.5	62.9	74.8
0.5	86.2 ± 2.8	38.9	39.3	88.6 ± 2.8	62.6	77.6

6.1.1. χ^2 statistic for the velocity fits

The likelihood statistic $\mathcal{L}$ does not by itself provide a measure of goodness of fit. WSDK and WS pointed out that it was not possible to construct a rigorous χ^2 statistic for their Tully-Fisher VELMOD fits because the distance and velocity errors were determined as part of likelihood maximization. This is not the case here, however, because (i) we have reliable distance errors for the Cepheid galaxies, and (ii) we have fixed the Cepheid velocity noise a priori (Eq. 19). Thus it makes sense to define and calculate a χ^2 statistic to test the goodness of fit of our velocity models to the Cepheid galaxy data.

We first define the expected distance in $\mathrm{km\,s^{-1}}$, or *Hubble flow distance,* given the redshift and the velocity model,

$$E(r|cz) = \frac{\int_0^\infty r^3 n(r) P(cz|r)\, dr}{\int_0^\infty r^2 n(r) P(cz|r)\, dr}\,, \tag{20}$$

along with the corresponding mean square distance

$$E(r^2|cz) = \frac{\int_0^\infty r^3 n(r) P(cz|r)\, dr}{\int_0^\infty r^2 n(r) P(cz|r)\, dr} \tag{21}$$

and distance error,

$$\delta r = \sqrt{E(r^2|cz) - [E(r|cz)]^2}\,. \tag{22}$$

The Cepheid distance in $\mathrm{km\,s^{-1}}$ is $H_0 d$, where d is the Cepheid distance in Mpc and H_0 is the best-fit Hubble constant for the model in question, and the corresponding error is $H_0 d\Delta$ (see §5.1). The χ^2 statistic measures the difference between $H_0 d$ and $E(r|cz)$ in units of the overall error:

$$\chi^2 = \sum_{i=1}^{27} \frac{(E(r|cz) - H_0 d)^2}{(\delta r)^2 + (H_0 d \Delta)^2}\,. \tag{23}$$

It is important to note that the Hubble flow contribution to the error, δr, is not determined solely by the velocity noise σ_v. Rather, it is the integrated effect of σ_v along the line of sight, taking into account the shape of the large-scale velocity field $u(r)$. In particular, in regions where $u'(r) < 0$ the effect of velocity noise is enhanced, creating comparatively large δr (see Appendix A of WS for further discussion).

The fourth and seventh columns of Table 7 list the χ^2 values for the Virgo-collapsed and uncollapsed fits. There are 26 degrees of freedom for the fit—27 galaxies minus one free parameter—so that the expected χ^2 value is 26, with rms dispersion $\sqrt{52} = 7.2$. The Virgo-collapsed fits with $\beta \geq 0.3$ thus have χ^2 values within $2\,\sigma$ of their expected values. These fits are therefore statistically acceptable, albeit with a larger χ^2 than desirable.

Two points are worth bearing in mind with regard to this statement, however. First, the relatively high χ^2 value is largely due to the influence of one galaxy, NGC 1326A, which deviates from the fit by $\sim 3\,\sigma$. When this object is excluded the computed χ^2 is well within $1\,\sigma$ of the expectation.[10] Second, the absolute value of χ^2 is strongly dependent on our adopted $\sigma_v(r)$. We chose $\sigma_v(r)$ similar to, though somewhat larger than, the value found by WS for a Tully-Fisher sample. If we take $\sigma_v(r) = 185\ \mathrm{km\,s^{-1}}$, the value indicated by the SBF fit (§5.3), we obtain $\chi^2 = 29.9$ for the $\beta = 0.4$ fit, fully compatible with expected value of 26 ± 7.2. (The best-fit Hubble constant rises to $86.8\ \mathrm{km\,s^{-1}\,Mpc^{-1}}$ for this choice of $\sigma_v(r)$, a change of less than $1\,\sigma$.) We believe that the smaller $\sigma_v(r)$ is appropriate for the late-type Cepheids, but this example shows that it is difficult to assign unambiguous significance to our χ^2 statistic. However, the statement that *the SBF-constrained IRAS models provide satisfactory fits to the Cepheid sample for* $\beta = 0.3$–0.5 is a reasonable one in view of the above discussion.

[10]Moreover, NGC1326A has very little effect on the value of H_0; for $\beta = 0.4$ we find $H_0 = 84.2\ \mathrm{km\,s^{-1}\,Mpc^{-1}}$ when NGC1326A is excluded.

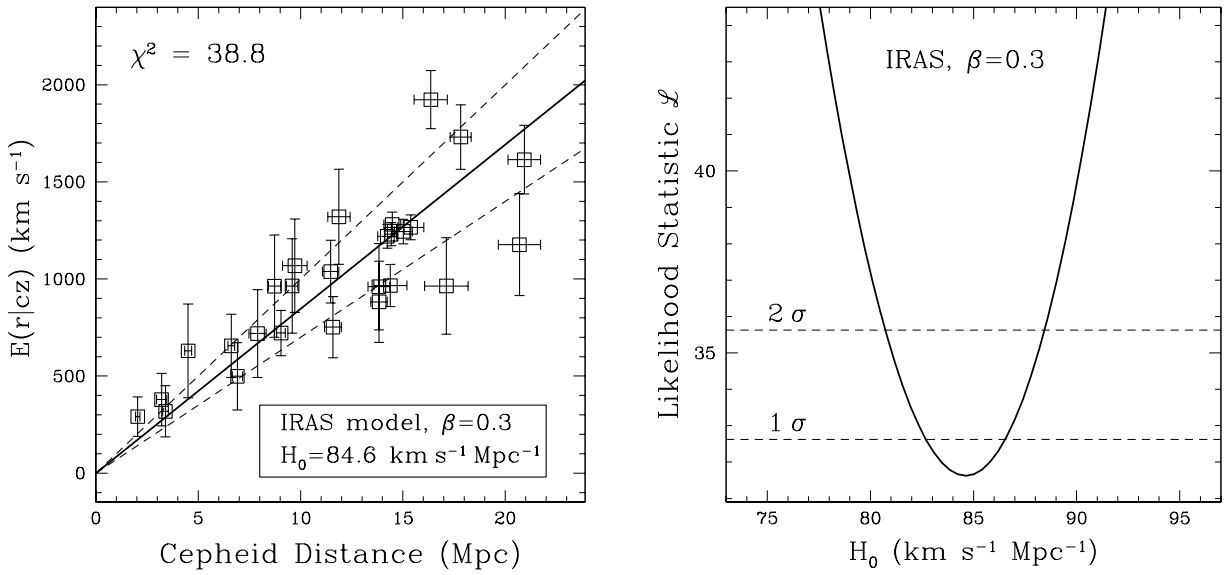

Fig. 6.— Hubble diagram for 27 Cepheid galaxies. The velocity model used is the IRAS $\beta = 0.3$ linear reconstruction; the expected distances in velocity units, $E(r|cz)$, are plotted versus the Cepheid distances in Mpc. The heavy solid line shows the best fitting Hubble constant, $H_0 = 84.6$ km s^{-1} Mpc^{-1}. The flatter dashed line is $H_0 = 70$ km s^{-1} Mpc^{-1}, and the steeper dashed line is $H_0 = 100$ km s^{-1} Mpc^{-1}.

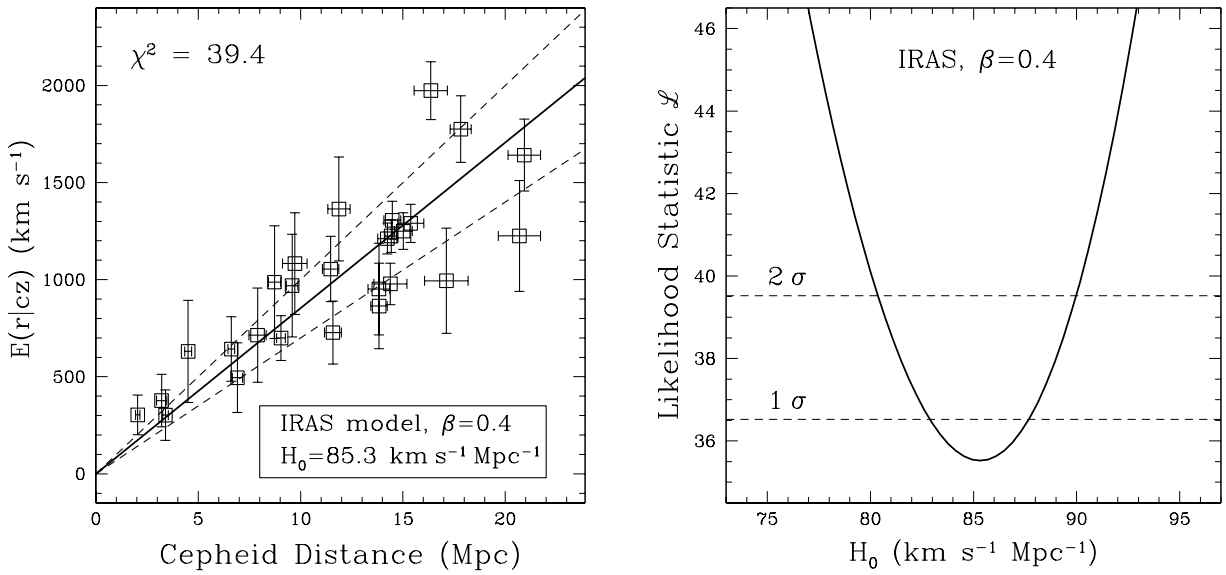

Fig. 7.— Same as the previous figure, but for an IRAS model with $\beta = 0.4$.

6.1.2. Hubble diagrams and confidence intervals

To assess the quality of the fits and the derived values of H_0, we plot Hubble diagrams in the left hand panels of Figures 6 and 7. The abcissa is the quantity $E(r|cz)$, the expected value of the Hubble flow distance given the LG frame redshift and the IRAS velocity model, as defined by Eq. (20). The vertical error bars are

the quantity δr defined by Eq. (22), and the horizontal error bars are the Cepheid distance uncertainty $d\Delta$. (We have approximated all errors as being symmetric.) In each Hubble diagram we plot the best-fit value of H_0 as a solid line through the points, with dashed lines representing the values $H_0 = 70\ \mathrm{km\,s^{-1}\,Mpc^{-1}}$ and $H_0 = 100\ \mathrm{km\,s^{-1}\,Mpc^{-1}}$ for comparison.

The diagrams validate the values of H_0 given in Table 7. The solid lines represent a far better fit to the majority of the data points than do the dashed lines drawn for comparison. The cluster of points very near the best fit Hubble line at a distance of 15 Mpc are the five collapsed Virgo galaxies. Their error bars are much smaller because we assume a velocity uncertainty of only $30\ \mathrm{km\,s^{-1}}$ for these objects, associated with the uncertainty in the Virgo redshift. (The error bars are, however, larger than $30\ \mathrm{km\,s^{-1}}$ because of the interaction between σ_v and $u(r)$ mentioned above.) It is evident from the diagrams that the fits are not perfect, with larger deviations being seen at the distance of Virgo. This may represent significant departures from the IRAS model in dense regions, a topic we further discuss in §7.1. As noted above, however, our uncertainty about the precise value of $\sigma_v(r)$ means we cannot state with assurance that these points do not fit the model.

The Hubble constant errors we have quoted are calculated by calculating the likelihood statistic $\mathcal{L}$ for a range of values of H_0 near the best fit value. (We hold all velocity field parameters, as well as $\sigma_v(r)$, constant as we vary H_0.) As discussed in detail by WSDK, $\mathcal{L}$ has the property that, when one fit parameter is varied, increases of $\Delta\mathcal{L} = \pm 1$ with respect to the minimum yield the $1\,\sigma$ errors on the parameter, while increases of $\Delta\mathcal{L} = \pm 4$ yield the $2\,\sigma$ errors. This is strictly true if the likelihood is Gaussian, or, equivalently, if the variation of $\mathcal{L}$ is parabolic near its minimum. This is a good approximation in the present case. The right hand panels of Figures 6 and 7 plot $\mathcal{L}$ versus H_0 for the $\beta = 0.3$ and $\beta = 0.4$ models respectively. The horizontal dashed lines show the 1 and $2\,\sigma$ confidence intervals on H_0 as determined by the procedure described above. These curves are the origin of the 95% confidence interval on H_0 of $5\ \mathrm{km\,s^{-1}\,Mpc^{-1}}$ quoted in the Abstract.

6.2. Results from the Tonry Model

We apply the phenomenological Tonry model to the Cepheid galaxies using the best-fit parameters arising from the SBF velocity fit. We again collapse Virgo in the Cepheid fit. We now fix the baseline velocity noise to $\sigma_v(r) = 150\ \mathrm{km\,s^{-1}}$, allowing it to rise to the SBF values in the cores of the model's attractors. The baseline noise is a bit higher than was the case for the IRAS fit (Eq. 19). However, the density dependence of $\sigma(r)$ for IRAS was such that non-cluster galaxies have very nearly the same velocity noise for the IRAS and Tonry model fits. The value of H_0 exhibits slight sensitivity to the value of σ_v, but the variation is small relative to the statistical errors.

Figure (8) shows the Hubble diagram resulting from fitting the Tonry model to the Cepheid data (left panel), along the likelihood versus H_0 curve (right panel). The maximum likelihood result find $H_0 = 91.8 \pm 1\ \mathrm{km\,s^{-1}\,Mpc^{-1}}$ at 65% ($1\,\sigma$) confidence. This is considerably larger, relative to the errors, than the result from the IRAS model. However, note that the χ^2 for the Tonry model fit, indicated on the Figure, is substantially larger than the value obtained for the IRAS fit.[11] Indeed, it deviates by more than $3\,\sigma$ from the expected value of 26. We conclude that the Tonry model is not an acceptable fit to the Cepheid distances; a corollary is that the discrepancy between the derived values of H_0 is not meaningful.

Note that the collapsed Virgo galaxies in the left panel of Figure 8 have vertical error bars that are

[11]The minimum value of the likelihood statistic $\mathcal{L}$ is also markedly larger than for the IRAS fit; however, the absolute likelihood statistics are not necessarily comparable for the two models owing to differences in implementation, such as the adoption of a constant density for the Tonry model.

much larger than those for the IRAS fit. This reflects the very strong Virgo infall inherent in the best-fit Tonry model—a triple-valued zone is produced near Virgo, which causes a small σ_v to translate in to a large δr. The large χ^2 for the fit probably indicates that the Tonry model attributes too much strength to the Virgo attractor as it attempts to compensate for the missing mass concentrations and voids that the IRAS model contains.

Table 8 lists the data plotted in Figures 6, 7 and 8.

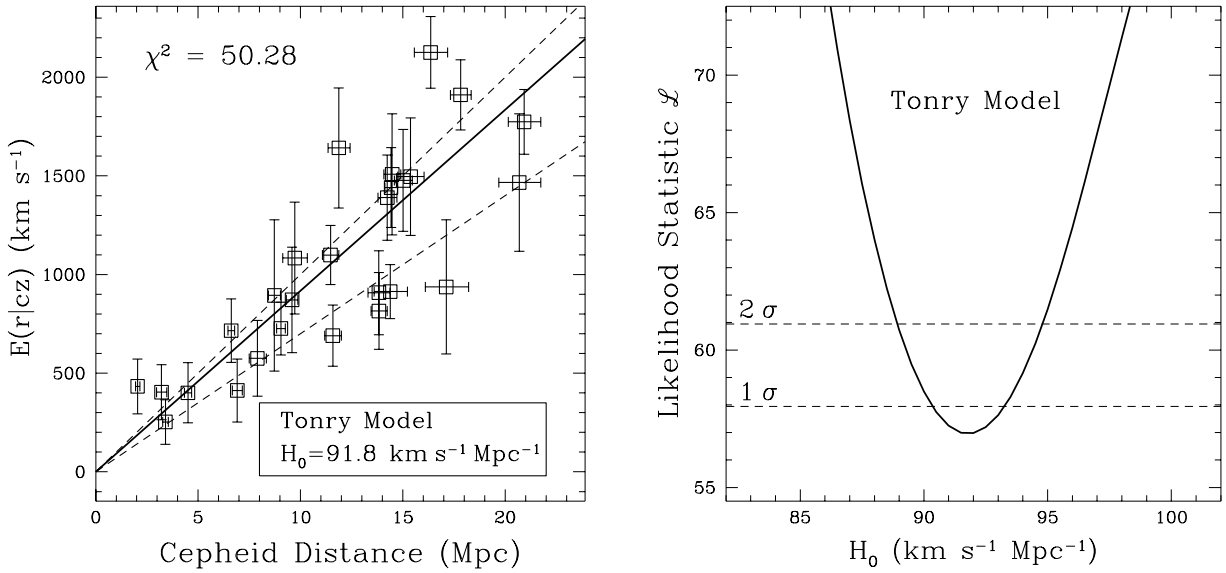

Fig. 8.— Same as the previous figures, but for the phenomenological Tonry model with $\sigma_v = 135$ km s^{-1}.

7. Discussion and Summary

We have argued in this paper that $H_0 = 85 \pm 5$ km s^{-1} Mpc^{-1} at 95% confidence, considering random error only. This result, if correct, leads to an expansion timescale $H_0^{-1} = 10.9$–12.2 Gyr, and thus an expansion age $t_0 = f(\Omega_{\rm m}, \Omega_\Lambda) H_0^{-1}$ that is shorter still (see the discussion in §1), unless $\Omega_{\rm m} = 1 - \Omega_\Lambda \lesssim 0.25$. For example, for $H_0 = 85$ km s^{-1} Mpc^{-1} and an $\Omega_{\rm m} = 0.3$, $\Omega_\Lambda = 0.7$ cosmology, $t_0 = 11.1$ Gyr. This expansion age may be compared with the estimated age of the oldest globular clusters, $t_* = 12.8 \pm 1$ Gyr ($1\,\sigma$ uncertainty; Krauss 1999). At first blush, then, our estimated Hubble constant leads to a universe younger than its oldest stars. Given this logical contradiction, our result obviously requires further scrutiny. We discuss a number of salient issues in this final section.

7.1. Why do we disagree with the H_0KP?

The H_0KP team reported $H_0 = 71 \pm 6$ km s^{-1} Mpc^{-1} (Mould et al. 2000). However, of their reported 9% ($1\,\sigma$) error, approximately 6.5% is systematic error due mainly to uncertainty in the distance to the LMC. This systematic error affects our value in precisely the same way as theirs, and thus should not be considered in comparing our H_0 estimates. The $1\,\sigma$ *random* error in the H_0KP Hubble constant is ~ 4.4 km s^{-1} Mpc^{-1}, corresponding to a $2\,\sigma$ error of ~ 9 km s^{-1} Mpc^{-1}. Thus, the H_0KP estimate overlaps with ours only at the very edges of our respective $2\,\sigma$ error bars (i.e., at 80 km s^{-1} Mpc^{-1}). Since we have used the same

Table 8. Plotted Data

Name	d (Mpc)	$cz_{\rm CMB}$ ($\rm km\,s^{-1}$)	$E(r\|cz)$ IRAS $\beta = 0.3$ ($\rm km\,s^{-1}$)	$E(r\|cz)$ IRAS $\beta = 0.4$ ($\rm km\,s^{-1}$)	$E(r\|cz)$ Tonry Model ($\rm km\,s^{-1}$)
NGC 3031	3.40 ± 0.14	46	319 ± 132	325 ± 122	224 ± 100
NGC 300	2.04 ± 0.11	-89	291 ± 101	206 ± 74	411 ± 127
NGC 5457	6.91 ± 0.25	360	499 ± 174	549 ± 164	378 ± 143
NGC 5253	3.21 ± 0.25	678	379 ± 135	299 ± 109	369 ± 133
NGC 4258	7.90 ± 0.42	651	719 ± 226	771 ± 223	378 ± 126
NGC 4548	15.38 ± 0.64	805	1270 ± 60	1460 ± 60	541 ± 169
NGC 925	9.04 ± 0.21	326	722 ± 116	733 ± 95	1500 ± 300
NGC 2541	11.58 ± 0.41	694	752 ± 157	831 ± 134	675 ± 142
NGC 3198	13.84 ± 0.39	879	882 ± 209	953 ± 197	793 ± 178
NGC 4414	17.13 ± 1.06	988	964 ± 248	1040 ± 250	866 ± 312
NGC 3621	6.62 ± 0.16	1059	656 ± 163	568 ± 141	700 ± 147
NGC 3627	8.73 ± 0.30	1072	963 ± 263	996 ± 274	815 ± 351
NGC 3319	13.83 ± 0.53	978	960 ± 222	1040 ± 210	884 ± 195
NGC 3351	9.59 ± 0.28	1123	964 ± 243	988 ± 244	821 ± 235
NGC 7331	14.39 ± 0.82	492	966 ± 109	1010 ± 80	905 ± 124
NGC 3368	9.72 ± 0.60	1242	1070 ± 240	1110 ± 240	1050 ± 270
NGC 2090	11.47 ± 0.40	1002	1040 ± 160	957 ± 140	1090 ± 135.3
NGC 4639	20.69 ± 1.03	1328	1180 ± 262	1250 ± 270	1460 ± 340
NGC 4725	11.87 ± 0.54	1486	1320 ± 240	1450 ± 253	1640 ± 290
NGC 1425	20.93 ± 0.79	1413	1610 ± 180	1560 ± 170	1770 ± 150
NGC 4321	14.48 ± 0.41	1893	1280 ± 60	1480 ± 60	1510 ± 310
NGC 1365	17.83 ± 0.51	1539	1730 ± 170	1690 ± 150	1900 ± 170
NGC 4496A	14.43 ± 0.30	2070	1230 ± 60	1340 ± 80	1440 ± 200
NGC 4536	14.24 ± 0.47	2148	1220 ± 60	1310 ± 70	1390 ± 220
NGC 1326A	16.36 ± 0.81	1730	1920 ± 150	1900 ± 130	2120 ± 170
NGC 4535	15.02 ± 0.43	2293	1240 ± 60	1400 ± 70	1470 ± 260

Cepheid data set to arrive at our estimates, and therefore share much of their random error, this constitutes a significant disagreement.

There are two principal causes of this disagreement. The first is the difference in Cepheid calibration as discussed in §3. Our OGLE-based PL calibration produces distances that are smaller by $\sim 5\%$ on average, primarily because the OGLE calibration yields larger reddening and thus larger extinction estimates. When applied to the H_0KP distances and their procedure for estimating the Hubble constant, the OGLE calibration should bring their value up to $\sim 75\ \mathrm{km\,s^{-1}\,Mpc^{-1}}$, closer to the value we derive, though still inconsistent, given that we use the same data.

The second source of disagreement is more fundamental: the different strategies we have adopted for determining H_0. The H_0KP approach (referred to as "Method I" in §2) has been to use the Cepheid galaxies as calibrators for secondary distance indicators (DIs), especially Type Ia Supernovae (SN Ia), the Tully-Fisher and Fundamental Plane relations, and the SBF relation. The secondary DIs are then applied to galaxies at much larger distances than the Cepheid galaxies themselves, typically in the 3000–$10,000\ \mathrm{km\,s^{-1}}$ range, where peculiar velocities can be largely neglected. In contrast, we have derived H_0 from the Cepheid galaxies themselves, correcting the effects of non-Hubble motions with velocity field models ("Method II" of §2).

The two strategies are subject to different pitfalls. Method I can go awry with the propagation of Cepheid errors into the calibration of the secondary DIs. Such errors might occur for a variety of reasons, the foremost being the difficult nature of the measurements. SN Ia are often historical, i.e., occurred many years or decades ago, and the data on their brightnesses may not be consistent with modern methods. And yet, such historical SN Ia must be used in the calibration procedure, SN Ia being rare events and Cepheid galaxies being few in number. Four out of six SN Ia calibrated by Gibson et al. (2000) occurred prior to 1990, and two of these occurred prior to 1975. This small sample of calibrators introduces the biggest uncertainty in the SN-based H_0 (Suntzeff et al. 1999). The calibration of the SBF and Fundamental Plane (FP) methods suffer from another problem: Cepheids are found in late-type spiral galaxies, whereas SBF applies best, and FP applies only, to early type galaxies. Consequently, the absolute calibration of the FP relation using Cepheid distances (Kelson et al. 2000) must be obtained indirectly, by assuming that the Cepheid calibrators and the FP ellipticals are members of a group lying at a common distance. The SBF relation has been calibrated using a small number of spirals with prominent bulges (Ferrarese et al. 2000a), but possible stellar population differences between spiral bulges and ellipticals make the validity of this calibration uncertain (Tonry et al. 1997; TBAD00).

Neither of the above problems applies to the H_0KP calibration of the Tully-Fisher relation by Cepheid galaxies (Sakai et al. 2000). However, Sakai et al. obtained their value of H_0 from a single I band Tully-Fisher data set, that of Giovanelli and collaborators (e.g., Giovanelli et al. 1997). Although this data set is of high quality, there are a number of other large Tully-Fisher data sets of recent vintage that were not considered by Sakai et al., such as those collected in the the Mark III Catalog (Willick et al. 1997a). Tully-Fisher measurements are prone to systematic differences in velocity width and photometric measurement conventions, and application of the Cepheid-calibrated Tully-Fisher relation to a wider range of Tully-Fisher data sets is needed; an important first step in this direction has been taken by Tully & Pierce (1999).

A coincidence of multiple secondary DI miscalibrations is very unlikely, at best. Nevertheless, our Method II analysis does not involve secondary DI's and cannot suffer from the problem of propagated Cepheid calibration errors.[12] However, our approach is vulnerable to inaccurately modeled peculiar velocities because we measure H_0 locally (see the discussion in §2). Our peculiar velocity models are "state-of-the-art,"

[12]It does, of course, potentially suffer from calibration error in the Cepheid PL relation, but this is essentially the problem of the LMC distance.

especially the IRAS models, and we have optimized them with respect to the SBF data set, which is the best current sample for constraining the local velocity field. It is evident from our Hubble diagrams, however, that our velocity models are not perfect. A clear indication of this is the ridge of ~ 5 galaxies that lie well below our best-fit Hubble line in Figures 6 and 7. These are objects that lie within, and in the background of, the Virgo-Ursa Major region, and that are falling in toward Virgo or Ursa Major at higher velocity than predicted by the model. None of these objects deviates from our model at more than the $2\,\sigma$ level—indeed, the only $3\,\sigma$ deviant point is NGC 1326A, which is above the $H_0 = 100\ \mathrm{km\,s^{-1}\,Mpc^{-1}}$ line at a distance of 16.4 Mpc—but it is still disquieting to see the large scatter at distances near and beyond Virgo. This scatter does not invalidate our approach, but reminds us that peculiar velocities are not fully accounted for in our model, and that some caution is needed in interpretation.

7.2. Considerations for future work

The discussion above shows that the debate on the Hubble constant will continue. Its ultimate resolution will require that several key needs are met:

1. *More nearby galaxies with accurate Cepheid distances.*— Our local measurement of H_0 could be greatly improved with a larger, and more uniformly distributed, sample of Cepheid galaxies. It is to be hoped that further observations by the HST, and later by NGST, will yield such samples. Indeed, such measurements would enable a better grasp of the systematic error in Method II values of H_0, along the lines of an angular variance analysis suggested by Turner, Cen & Ostriker (1992).

2. *Improved models for the local velocity field.*— The IRAS model presented here is a reasonable but imperfect fit to both the SBF and the Cepheid distances. Work is currently under way by WNSB to test enhancements of the model. In particular, we intend to further investigate the effects of nonlinear dynamics and nonlinear bias. Another dynamical variable that needs to be better understood is the small-scale velocity noise and its dependence on galaxy density. If these efforts succeed, the uncertainty in H_0 due to peculiar velocities will be reduced.

3. *A re-calibration of secondary DIs.*— As noted in §2, both the "distant" and "local" strategies for measuring H_0 should be pursued, and eventually they should agree. We have pointed to a few issues where the H_0KP calibrations of secondary DIs could contain subtle errors. For further investigation, one could use the Cepheid distances to calibrate the Tully-Fisher relations for samples not considered by Sakai et al. 2000, in particular, those tabulated in the Mark III Catalog (Willick et al. 1997a), especially after possible calibration errors in that and other catalogs have been corrected via comparison with the uniform, all-sky Shellflow survey recently presented by Courteau et al. (2000).

4. *Further exploration of the "Hubble bubble".*— The approach of this paper, and, to a lesser extent, that of the H_0KP, could overestimate the Hubble constant if the local universe ($d \lesssim 30h^{-1}\,\mathrm{Mpc}$) is expanding more rapidly than the global average, as has been suggested by Zehavi et al. (1998) on the basis of SN Ia data within $\sim 10,000\ \mathrm{km\,s^{-1}}$. Such a situation is certainly possible on theoretical grounds; a fractional mass fluctuation δ_M within a sphere of radius R produces a deviation of the Hubble constant within that sphere of $\delta H_0/H_0 \approx -\Omega_{\mathrm{m}}^{0.6}\delta_M/3$ (see Turner, Cen & Ostriker 1992 and Tomita 2000 for more detailed theoretical analyses). Typical mass fluctuations on scales $R \gtrsim 10h^{-1}\,\mathrm{Mpc}$ are $\lesssim 1$ in most cosmological scenarios, so that one would expect that the local value of H_0 on a $\sim 10\,h^{-1}\,\mathrm{Mpc}$ scale to deviate by $\sim$ 10–20% from the global value if $\Omega_{\mathrm{m}} \approx 0.3$, with smaller deviations on larger scales. However, for our local value of H_0 to *exceed* the global value, it would be necessary for our local neighborhood to be *underdense* relative to the mean. And yet, the 1.2 Jy IRAS density field suggests that the opposite is true—our local region within 20 Mpc is overdense relative to the volume within 100 Mpc well that is well-sampled by IRAS. Moreover, recent Tully-Fisher data (Dale & Giovanelli

2000) do not support the claim of Zehavi et al. (1998) for a local Hubble bubble. It is prudent to view this issue as an open one for now, and to continue to test the relationship between the local and distant Hubble flow. Such tests do not require DIs that are absolutely calibrated, and thus are independent of the question of H_0 itself.

5. *More accurate absolute calibration of the PL relation.*— As discussed in §2, the largest systematic error in the analysis of this paper is due to uncertainty in the zero point of the Cepheid PL relation, which is itself due to uncertainty in the distance to the LMC. We have adopted the "canonical" value $\mu_{\rm LMC} = 18.50$ in this paper, the same as that adopted by the H_0KP. Our H_0 estimate could be range between 78 and 98 $\rm km\,s^{-1}\,Mpc^{-1}$ depending on the distance to the LMC chosen.

It is, finally, worth taking a moment to consider the question, What if H_0 really is as large as, say, 90 $\rm km\,s^{-1}\,Mpc^{-1}$? Would that constitute a "crisis for Big Bang cosmology," a claim that has been heard in some quarters? The answer, for the moment, is clearly "No," for two reasons. First, the globular clusters could still be as young as $t_* = 10$ Gyr. Such a young age is unlikely but possible at the few percent level (Krauss 1999). If this were the case, then $t_0 > t_*$ for $H_0 = 90$ $\rm km\,s^{-1}\,Mpc^{-1}$ and $\Omega_{\rm m} = 0.3$, $\Omega_\Lambda = 0.7$. One would then require only that the globular clusters formed very shortly ($\lesssim 10^8$ yr) after the Big Bang, which is not impossible. Second, even if $t_* = 13$ Gyr is correct, one can obtain $t_0 \geq t_*$ for $H_0 = 90$ $\rm km\,s^{-1}\,Mpc^{-1}$ if $\Omega_{\rm m} = 1 - \Omega_\Lambda \leq 0.13$. A universe of such low density has not been ruled out. In short, a Hubble constant ≈ 90 $\rm km\,s^{-1}\,Mpc^{-1}$ does not pose an insurmountable problem for Big Bang cosmology so long as the ages of the oldest stars and the values of the parameters $\Omega_{\rm m}$ and Ω_Λ remain poorly determined.

7.3. Summary

We have presented a new determination of the Hubble constant using Cepheid PL data published by the H_0KP. Rather than use the nearby ($d \lesssim 20$ Mpc) Cepheid galaxies as calibrators for secondary distance indicators, which are then applied to more distant ($d \gtrsim 50$ Mpc) galaxies for which peculiar motions are fractionally small (the H_0KP strategy), we use Cepheid galaxies directly to measure H_0.

We first redetermined the Cepheid galaxy distances using a calibration of the PL relation derived from a large sample of LMC Cepheids presented by the OGLE group. Our absolute PL calibration assumed $\mu_{\rm LMC} = 18.5$. (We reemphasize that the H_0KP group will shortly present their own revision of Cepheid distances in light of the OGLE LMC Cepheid data [Madore & Freedman 2000, in preparation; Freedman et al. 2000, in preparation].) We then presented two models of the local peculiar velocity field. The first was obtained from the IRAS galaxy density field using the linear relation between large-scale velocity and density fields and the assumption that IRAS galaxies trace the mass density field up to a linear biasing factor b. The IRAS model applies in the Local Group reference frame. The second was the phenomenological model of TBAD00, which applies in the CMB reference frame. The Tonry model assumes the local velocity field is dominated by infall to the Virgo and Great Attractors, along with a dipole and quadrupole term. We optimized each model by fitting it, using the maximum likelihood VELMOD algorithm of WSDK and WS, to a calibration-free 281-galaxy subset of the SBF sample of Tonry et al. (2001), currently the most accurate set of relative-distances for galaxies in the nearby ($cz \lesssim 3000$ $\rm km\,s^{-1}$) universe. In the case of the IRAS model, this optimization consisted mainly of determining the value of $\beta = \Omega_{\rm m}^{0.6}/b$, which was found to be 0.38 ± 0.06 ($1\,\sigma$ error), with $0.2 \leq \beta \leq 0.5$ allowed at the $3\,\sigma$ level. For the Tonry model the optimization involved constraining several parameters that determine the influence of the Virgo and Great Attractors. The velocity model fits used only relative distances for the SBF galaxies and thus in no way prejudiced our subsequent determination of H_0.

We then applied the IRAS and Tonry velocity models to 27 Cepheid galaxies, again using the VELMOD algorithm, with the one remaining free parameter now being the Hubble constant. This yielded $H_0 =$

85 ± 5 km s^{-1} Mpc^{-1}, essentially independent of the value of β, when the IRAS velocity field was used. When the Tonry model was used we obtained $H_0 = 92 \pm 5$ km s^{-1} Mpc^{-1}. The quoted random errors are at the 95% confidence level. The IRAS model produced a better fit likelihood than the Tonry model, and a Hubble diagram with markedly less scatter. We thus favor the result from IRAS, and adopt the IRAS value of H_0 for our final conclusion. This value is significantly larger than the H_0KP result, $H_0 = 71 \pm 6$ km s^{-1} Mpc^{-1} (Mould et al. 2000).

Until Method I and Method II analyses give consistent results, we find it untenable to state that H_0 is known to within 10%. We discussed at length in §7.1 several possible reasons for the difference, as well as (§7.2) a number of lines of further investigation needed to clarify the issue. Should the larger value we quote here turn out to be correct, it would be difficult to reconcile the expansion age of the universe, $t_0 = 11.1$ Gyr for $\Omega_{\rm m} = 0.3$, $\Omega_\Lambda = 0.7$, with the estimated ages of oldest globular clusters, 12.8 ± 1 Gyr (Krauss 1999). However, the remaining uncertainty in these stellar ages, as well as in the cosmological density parameters, is sufficiently large that a Hubble constant as large or even somewhat larger than what we have argued for here does not yet pose a logical inconsistency for Big Bang cosmology.

Sadly, Jeff died in a car accident only two days after we (PB and JAW) first huddled over the APJ referee's report. I'd like to think that some part of Jeff's wisdom shows in my own halting revisions to this paper. I would like to thank Stephane Courteau & Michael Strauss for helping with the completion of this work; I am also grateful for Tod Lauer's referee's report. I would have liked to thank JAW for his time—so valuable to me now. Jeff's original acknowledgements follow below.

This paper would not have been possible without the generous assistance of a number of individuals who shared data and expertise. We are particularly grateful to Wendy Freedman for timely input regarding the evolving calibration of the PL relation and helpful comments on an initial draft of this paper. H_0KP team members Laura Ferrarese and Brad Gibson also provided useful input on calibration issues. In addition, we acknowledge the entire H_0KP team for their epochal achievement in putting together the HST Cepheid database. Pierre Lanoix is thanked for his efforts in assembling and maintaining the Extragalactic Cepheid Database. Jeff Newman kindly provided his Cepheid data for NGC 4258 in advance of publication. Special thanks are due to Vijay Narayanan and Michael Strauss for producing IRAS-predicted peculiar velocities and densities used in this paper, and for helpful comments on the paper. Finally, we owe a large debt to John Tonry and his collaborators for their fine SBF data set, which enabled us to constrain the local velocity field. We are particularly grateful to John Blakeslee who shared the SBF data, and his wisdom on how to use it, with us prior to its publication.

JAW was supported by a Cottrell Scholarship of Research Corporation and a Terman Fellowship from Stanford University, and, during the initial phase of this work, NSF grant AST96-17188.

A. Calculation of random distance errors

Although the systematic zero point errors in the Cepheid PL relation dominate the distance error budget, the weights we assign to the galaxies in the Hubble constant fit must be determined by random error only. To calculate this error we must account for how PL scatter couples with the reddening determination. The result of this coupling is that the distance error is markedly larger than one might naively expect.

We denote the I and V band galaxy (random) distance modulus errors $\delta\mu_I$ and $\delta\mu_V$. These errors are due to PL scatter, and we assume them to be distributed as Gaussian random variables with mean zero and rms dispersions $\sigma_I/\sqrt{N_{\rm Ceph}}$ and $\sigma_V/\sqrt{N_{\rm Ceph}}$, where σ_I and σ_V are the I and V band rms PL scatter. The modulus errors induce an error $\delta(V-I) = \delta\mu_V - \delta\mu_I$ in the mean $(V-I)$ color, which leads in turn to an

error in the assumed reddening given by

$$\delta E(B-V) = \frac{\delta(V-I)}{R_V - R_I}\,, \tag{A1}$$

where the $R_X \equiv A_X/E(B-V)$ are given in Table 2. The corresponding error in the distance modulus we assign to the galaxy is

$$\delta\mu^{red} = -\frac{1}{2}\,(R_V + R_I)\,\delta E(B-V) = -\frac{1}{2}\,\frac{R_V + R_I}{R_V - R_I}\,\delta(V-I)\,, \tag{A2}$$

where we have assumed that the V and I band data are equally weighted in the distance determination, as they are in the present application. The negative sign in Eq. (A2) arises because PL errors that make the galaxy appear redder result in its being *overcorrected* for extinction, i.e., assigned too small a distance modulus.

Eq. (A2) represents only that part of the distance modulus error due to reddening determination error. To it we must add the direct error due to PL scatter, $\delta\mu^{direct} = (\delta\mu_V + \delta\mu_I)/2$. Adding the two, and writing the result in terms of the independent variables $\delta\mu_V$ and $\delta\mu_I$, we obtain the overall galaxy distance modulus error,

$$\delta\mu = \frac{1}{2}\left[(1-\Delta_f)\,\delta\mu_V + (1+\Delta_f)\,\delta\mu_I\right]\,, \tag{A3}$$

where we have defined

$$\Delta_f \equiv \frac{R_V + R_I}{R_V - R_I} = 4.0625\,. \tag{A4}$$

The numerical value of Δ_f follows from the values of R_V and R_I in Table 2. Eq. (A3) tells us that $\delta\mu$ is normally distributed with mean zero and rms dispersion

$$\sigma_\mu = \sqrt{\left(\frac{1-\Delta_f}{2}\right)^2 \sigma_V^2/N_{\rm Ceph} + \left(\frac{1+\Delta_f}{2}\right)^2 \sigma_I^2/N_{\rm Ceph}}\,. \tag{A5}$$

If we furthermore take $\sigma_V \approx \sigma_I = \sigma_{\rm Ceph}$, the last equation reduces to

$$\sigma_\mu = \frac{\sigma_{\rm Ceph}}{2\sqrt{N_{\rm Ceph}}}\,\sqrt{(1-\Delta_f)^2 + (1+\Delta_f)^2} = 2.96\,\frac{\sigma_{\rm Ceph}}{\sqrt{N_{\rm Ceph}}}\,. \tag{A6}$$

The corresponding expression for the rms error in the mean reddening for the galaxy is

$$\sigma_{E(B-V)} = \frac{\sqrt{2}}{R_V - R_I}\,\frac{\sigma_{\rm Ceph}}{\sqrt{N_{\rm Ceph}}} = 1.1\,\frac{\sigma_{\rm Ceph}}{\sqrt{N_{\rm Ceph}}}\,. \tag{A7}$$

We use Eqs. (A6) and (A7), with $\sigma_{\rm Ceph} = 0.15$ mag, to calculate the distance modulus and reddening errors in columns 2 and 4 of Table 5. (The distance errors in column 3 are computed directly from the modulus errors in the standard fashion.)

REFERENCES

Batra, P. & Willick, J.A. 2000, "A Direct Cepheid Measurement of H_0," to appear in Proceedings of the XXXVth Rencontres de Moriond: Energy Densities in the Universe

Berlind, A.A., Narayanan, V.K., & Weinberg, D.H. 2000, ApJ, 537, 537

Blakeslee, J.P., Davis, M., Tonry, J.L., Dressler, A., & Ajhar, E.A. 1999, ApJ, 527, L73

Caretta, E., Gratton, R.G., Clementini, G., & Fusi Pecci, F. 2000, ApJ, 533, 215

Cioni, M.-R. L., van der Marel, R.P., Loup, C., & Habing, H.J. 2000, AA 359, 601

Courteau, S. & van den Bergh, S. 1999, AJ, 118, 337

Courteau, S., Willick, J.A., Strauss, M.A., Schlegel, D., & Postman, M. 2000, ApJ, 544, 636

Dale, D.A., & Giovanelli, R. 2000, in ASP Conf. Ser. 201, Cosmic Flows Workshop, ed. S. Courteau, M.A. Strauss, & J.A. Willick (San Fransisco: ASP), 25

Davis, M., Nusser, A., & Willick, J. A. 1996, ApJ, 473, 22

Ferrarese, L. et al. 2000a, ApJ, 529, 745

Ferrarese, L. et al. 2000b, in *Cosmic Flows 1999: Towards an Understanding of Large-Scale Structure,* eds. S. Courteau, M.A. Strauss, & J.A. Willick (ASP Conference Series)

Fisher, K.B., Huchra, J.P., Strauss, M.A., Davis, M., Yahil, A., & Schlegel, D. 1995, ApJS, 100, 69

Freedman, W.L. et al. 1992, ApJ, 396, 80

Gibson, B.K. 1999, astro-ph/9910574 (acceped in Mem. Soc. Astron. Ital.)

Gibson, B.K. et al. 2000, ApJ, 529, 723

Giovanelli, R., Haynes, M.P., Herter, T., Vogt, N.P., Wegner, G., Salzer, J.J., Da Costa, L.N., & Freudling, W. 1997, AJ, 113, 22

Kelson, D.D. et al. 2000, ApJ, 529, 768

Kepner, J.V., Summers, F.J., & Strauss, M.A. 1997, NewA, 2, 165

Lanoix, P., Garnier, R., Paturel, G., Petit, C., Rousseau, J., & Di Nella-Courtois, H. 1999a, Astron. Nachr. 320, 21

Lanoix, P., Paturel, G., & Garnier, R. 1999b, MNRAS, 308, 969

Herrnstein, J.R., et al. 1999, Nature, 400, 539

Hoyle, F., Shanks, T., & Tanvir, N.R. 2000, MNRAS, submitted (preprint astro-ph/0002521)

Huchra, J. 1985, in The Virgo Cluster, ed. O. Richter & B. Binggeli (Garching: ESO), 181

Krauss, L.M. 2000, Phys.Rept. 333-334 (David Schramm's Universe), 33

Lange, A.E. et al. 2000, astro-ph/0005004 (submitted to PRD)

Maoz, E. et al. 1999, Nature, 401, 351

Mateo, M. 1998, ARA&A, 36, 435

Mould, J.R. et al. 2000, ApJ, 529, 786

Popowski, P., & Gould, A. 1998, ApJ, 506, 259

Primack, J. et al. 2000, in ASP Conf. Ser. 201, Cosmic Flows Workshop, ed. S. Courteau, M.A. Strauss, & J.A. Willick (San Francisco: ASP), 389

Sakai, S. et al. 2000, ApJ, 529, 698

Saha, A., Sandage, A., Tamman, G.A., Labhardt, L., Macchetto, F.D., & Panagia, N. 1999, ApJ, 522, 802

Schlegel, D., Finkbeiner, D.P., & Davis, M. 1998, ApJ, 500, 525 [SFD]

Stanek, K.Z., Zaritsky, D., Harris, J. 1998, ApJ, 500 L141

Strauss, M.A., Huchra, J.P., Davis, M., Yahil, A., Fisher, K., & Tonry, J. 1992, ApJS, 83, 29

Strauss, M.A., Ostriker, J.P., & Cen, R. 1998, ApJ, 494, 20

Suntzeff, N.B. et al. 1999, AJ, 117, 1175 ApJ, 494, 20

Tanvir, N.R., Shanks, T., Ferguson, H.C., & Robinson, D.R.T. 1995, Nature, 377, 27

Tegmark, M. & Zaldarriaga, M. 2000, ApJ, 544, 30

Tomita, K. 2000, astro-ph/0005031

Tonry, J.L. & Schneider, D.P. 1988, AJ, 96, 807

Tonry, J.L., Blakeslee, J.P., Ajhar, E.A., & Dressler, A. 1997, ApJ, 475, 399

Tonry, J.L., Blakeslee, J.P., Ajhar, E.A., & Dressler, A. 2000, ApJ, 530, 625 (TBAD00)

Tonry, J.L. et al. 2001, 546, 681

Tully, R.B., & Pierce, M.J. 2000, ApJ, 533, 744

Turner, E.L., Cen, R., & Ostriker, J.P. 1992, AJ, 103, 1427

Udalski, A., Szymanski, M., Kubiak, M., Pietrzynski, G., Soszynski, I., Wozniak, P., & Zebrun, K. 1999a, Act. Astron., 49, 201

Udalski, A., Soszynski, I., Szymanski, M., Kubiak, M., Pietrzynski, G., Wozniak, P., & Zebrun, K. 1999b, Act. Astron., 49, 223

Willick, J. A., Courteau, S., Faber, S. M., Burstein, D., Dekel, A., & Strauss, M. A. 1997a, ApJS, 109, 333 (MarkIII)

Willick, J.A., Strauss, M.A., Dekel, A., & Kolatt, T. 1997b, ApJ, 486, 629 (WSDK)

Willick, J.A., & Strauss, M.A. 1998, ApJ, 507, 64 (WS)

Willick, J.A. 2000, "Cosmic Velocities 2000: A Review," to appear in Proceedings of the XXXVth Rencontres de Moriond: Energy Densities in the Universe (astro-ph/0003232)

Worthey, G. 1993, ApJ, 409, 530

Yahil, A. 1985, Workshop on the Virgo Cluster of Galaxies, ESO, Munich

Zehavi, I., Riess, A.G., Kirshner, R.P. & Dekel, A. 1998, ApJ, 503, 483

This preprint was prepared with the AAS LaTeX macros v5.0.